Assessing single-component gene drive systems in the mosquito *Aedes aegypti* via single generation crosses and modeling

William Reid[1§], Adeline E Williams[2,3§], Irma Sanchez-Vargas[2], Jingyi Lin[1], Rucsanda Juncu[1], Ken E Olson[2], Alexander WE Franz*[1]

[1]Department of Veterinary Pathobiology, University of Missouri, Columbia, MO 65211, USA.
[2]Department of Microbiology, Immunology, and Pathology, Colorado State University, Fort Collins, CO 80523, USA.
[3]Current address: Laboratory of Malaria and Vector Research, National Institute of Allergy and Infectious Diseases, National Institutes of Health, Rockville, MD, 20852, USA.

[§]Contributed equally
[*]Corresponding author franza@missouri.edu

Short running head: CRISPR/Cas9 gene drive in *Ae. aegypti*

Keywords: gene drive blocking indels, arbovirus, CRISPR, genomic position effect, population replacement

Preprint Server: BioRxiv doi: https://doi.org/10.1101/2021.12.08.471839. CC-BY-NC-ND 4.0 International license

This PDF file includes:

Main Text
Figures 1 to 6
Tables 1 to 4

ABSTRACT

The yellow fever mosquito *Aedes aegypti* is a major vector of arthropod-borne viruses, including dengue, chikungunya, and Zika. A novel approach to mitigate arboviral infections is to generate mosquitoes refractory to infection by overexpressing antiviral effector molecules. Such an approach requires a mechanism to spread these antiviral effectors through a population, for example, by using CRISPR/Cas9-based gene drive (GD) systems. Critical to the design of a single-locus autonomous GD is that the selected genomic locus be amenable to both GD and appropriate expression of the antiviral effector. In our study, we used reverse engineering to target two intergenic genomic loci, which had previously shown to be highly permissive for antiviral effector gene expression, and we further investigated the use of three promoters (*nanos, β2-tubulin,* or *zpg*) for Cas9 expression. We then quantified the accrual of insertions or deletions (indels) after single generation crossings, measured maternal effects, and assessed fitness costs associated with the various transgenic lines to model the rate of GD fixation. Overall, MGDrivE modeling suggested that when an autonomous GD is placed into an intergenic locus, the GD system will eventually be blocked by the accrual of GD blocking resistance alleles and ultimately be lost in the population. Moreover, while genomic locus and promoter selection were critically important for the initial establishment of the autonomous GD, it was the fitness of the GD line that most strongly influenced the persistence of the GD in the simulated population. As such, we propose that when autonomous CRISPR/Cas9 based GD systems are anchored in an intergenic locus, they temporarily result in a strong population replacement effect, but as GD-blocking indels accrue, the GD becomes exhausted due to the fixation of CRISPR resistance alleles.

Significance statement

For the purpose of population replacement, CRISPR/Cas9 based gene drives (GD) have been developed in *Anopheles* spp. and split GDs have been developed in *Ae. aegypti.* In our study, we developed autonomous GD in *Ae. aegypti* and positioned the drives in intergenic loci ideal for the expression of antiviral effector genes. Our results suggest that when the GD is placed into an intergenic locus, there is rapid introgression of the GD resulting in a transient population

68 replacement followed by loss of the drive as resistance alleles accrue. Fitness of the transgenic
69 lines and maternal deposition of CRISPR/Cas9 components were the major contributing factors
70 affecting the perseverance of the GD in our population models.

71

72 **INTRODUCTION**

73 The yellow fever mosquito *Aedes aegypti* is the principal vector of arthropod-borne viruses
74 (arboviruses) such as dengue, yellow fever, chikungunya, and Zika in tropical regions of the
75 world (1-3). Presently, the major strategy to control *Ae. aegypti* populations relies on the use of
76 *Bacillus thuringiensis* var *israelensis* (*Bti*) and chemical insecticides; however, these approaches
77 have led to multiple mechanisms of insecticide resistance, warranting the ongoing quest for
78 alternative methods of control (4-5). Novel approaches, including the incompatible insect
79 technique (IIT) using the intracellular parasite *Wolbachia* (6, 7) and transgenic mosquitoes
80 containing dominant lethal transgenes (RIDL, fsRIDL), have been tested in the field (8, 9). Other
81 promising technologies, including precision-guided sterile insect technique (pgSIT) have been
82 developed for the purposes of localized, confinable management of *Ae. aegypti* populations (10,
83 11). Another genetic control strategy, termed population replacement, aims at spreading an
84 antipathogen (*i.e.*, antiviral) effector through a targeted mosquito population. Antiviral
85 effectors, specifically those blocking dengue and Zika viruses in *Ae. aegypti*, have been
86 previously developed and tested (12-17). Linking an autonomous gene drive (GD) system to the
87 antiviral effector could lead to super-Mendelian inheritance of the transgene within the
88 targeted mosquito population (18). As a consequence, the proportion of the population
89 harboring the effectors would be increased, resulting in the emergence of mosquitoes refractory
90 to arbovirus transmission. For such a broad-scale population replacement approach, the GD
91 system needs to overcome several limitations, including: 1) the antiviral effector must provide
92 sufficient efficacy to render the targeted population refractory, 2) the inheritance of the GD
93 must be greater than any fitness cost associated with the GD, and 3) the GD must be able to
94 outpace the development of GD resistant alleles. GD systems utilizing a homing endonuclease
95 gene (HEG) based approach were initially proposed in 2003 and subsequently demonstrated in
96 2008 in *Anopheles gambiae* as a fully synthetic homing GD using the DNA cleaving intron-

97 encoded endonuclease I-SceI (19). The CRISPR/Cas9 system has been modified to allow for HEG-
98 based GDs in *Drosophila melanogaster* (20), along with several mosquito species including
99 *Anopheles stephensi* (21, 22), *An. gambiae* (23), and *Ae. aegypti* (10, 24). The HEG-based GD
100 developed in *Ae. aegypti* inserted itself into the *white* gene on chromosome 1 and contained a
101 single guide RNA (sgRNA)-expressing cassette that targeted the locus, along with an eGFP eye
102 marker as cargo (10).

103 Highly invasive GD systems are thought to carry substantial environmental risk since they are
104 not designed to self-eliminate or be confinable to a region. However, several systems have been
105 developed that would allow for their recall, including systems that destroy or overwrite the GD,
106 and more recently, a "biodegradable" self-eliminating GD system (25-28). Split-GD systems have
107 been developed for *Ae. aegypti*; by design – these GD systems are modelled to be self-limiting
108 or self-extinguishing (10, 24). Five different *Ae. aegypti* lines, each of which expressed Cas9
109 under the control of a different promoter (*i.e.*, *exuperantia*, *4nitro*, *trunk*, *nup50*, and *PUb*) were
110 used to drive *in trans* an sgRNA-expressing cassette positioned in the *white* gene (10, 29). The
111 work by Li *et al* (2020) demonstrated an efficient split GD system that was designed to be
112 confinable (10). Of major concern to the development of an autonomous GD system with an
113 associated genetically linked antipathogen effector is that the expression patterns for the HEG-
114 based GD and the antipathogen effector are spatio-temporally distinct from each other. That is,
115 the HEG-based GD is ideally active in the germline during early gametogenesis while the
116 antipathogen effector is ideally expressed in tissues associated with the pathogen in the
117 mosquitoes, such as in the female midgut. Therefore, the genomic locus for an autonomous
118 CRISPR/Cas9 GD must allow for both the expression of the GD as well as the antipathogen
119 effector. Multiple viral effectors have been developed and tested in *Ae. aegypti* (30), with these
120 effectors all being incorporated into the genome in a quasi-random fashion using transposons.
121 While multiple genomic loci have been identified to be suitable for transgene expression in *Ae.*
122 *aegypti*, two of our previous studies have identified genomic loci that reliably allow for high
123 levels of gene expression in the female midgut following ingestion of a blood meal (13, 31). In
124 our studies, midgut-specific transgenes were placed under control of the *carboxypeptidase A*
125 promoter and identified two genomic loci that exhibited strong transgene expression: 'Carb 109'
126 (C109) and 'TIMP-P4' (T4) (13, 31). In addition, the Carb109 locus was found to be highly stable

127 for more than 50 generations for a dengue virus type 2 (DENV2)-targeting inverted-repeat
128 effector and represents an ideal genomic locus for the insertion and expression of antiviral
129 effectors. In our study, we took a reverse engineering approach to design, build, and test
130 autonomous CRISPR/Cas9-based GD systems that position the GD at intergenic loci known to
131 allow for efficient transgene expression in the midgut and investigated three promoters/3'-UTR
132 for the expression of the Cas9 nuclease. Following establishment, we characterized the GD along
133 with fitness parameters of the GD harboring lines and modeled how they would behave as a
134 single release in a confined area. Overall, our study demonstrates the effects of placing an
135 autonomous GD system in an intergenic genomic locus and highlights the many variables that
136 ultimately affect transgenic population fixation in the context of GD performance.

137

138 **MATERIALS AND METHODS**

139 **Generation of cDNA constructs**

140 The constructs used for establishing the GD lines were prepared in three sequential steps: 1) an
141 'empty' gene drive destination vector containing the homology arms corresponding to the
142 destination locus (*i.e.*: TIMP-P4 or Carb109); 2) the NLS-Cas9 gene from the pHsp70 Cas9
143 plasmid (Addgene plasmid #46294 (32)) connected to the promoters and 3'-UTRs from the
144 *β2tubulin* (AAEL019894), *nanos* (AAEL012107), and *innexin-4* (*zpg*, AAEL006726) genes,
145 respectively, 3) the respective sgRNA targeting either the TIMP-P4 or the Carb109 locus under
146 control of the U6:3 snRNA promoter (AAEL017774).

147

148 *Construction of 'empty' destination vectors for the GD cassettes*

149 The 'empty' destination vector for the TIMP-P4 locus (Chr2:32138225) was constructed as
150 previously described for plasmid AeaeCFPT4 (**Table S6**) with the exception that the eCFP marker
151 was replaced with that of mCherry as a two-fragment Gibson assembly (17). The ORF of
152 mCherry was amplified using primers BR-100 and BR-101, while primers BR-98 and BR-99 were
153 used to amplify the full backbone of the destination vector minus the eCFP marker (**Table S5**).
154 The two PCR fragments were then assembled using the HiFi Gibson Assembly kit from NEB

155 (Waltham, MA) following the manufacturer's instructions. The 'empty' destination vector for the
156 Carb109 locus (3: 409699138) was constructed by first amplifying the 459 bp upstream
157 homology arm (genomic positions AaegL5_3:409698681-409699140) using primers BR-368 and
158 BR-122, followed by insertion of the amplicon into pBluescript using *Kpn*I and *Xho*I. The 541 bp
159 downstream homology arm (genomic positions AaegL5_3: 3:409699139-409699680) was then
160 amplified using primers BR-113 and BR-364, followed by insertion of the amplicon into the
161 previous intermediate plasmid using *Xho*I and *Sac*II. Finally, the 3xP3-mCherry-SV40 cassette
162 was amplified from the empty TIMP-P4 destination vector using primers BR-54 and BR-55 and
163 cloned into the destination vector using *Xho*I followed by screening for orientation using primers
164 BR-60 and BR-54.

165

166 *Construction of the β2tubulinCas9 cassette*

167 The basic components of the β2tubulinCas9 construct were assembled in pUC19 in three steps.
168 First, the *β2tubulin* promoter/5'-UTR (AaegL5_2: 326339137-326338047) fragment was
169 amplified from the *Ae. aegypti* genome (HWE strain) using primers BR-32 and BR-33 and cloned
170 into pUC19 using *Hind*III and *Pst*I, which introduced an *Xho*I site upstream of the promoter and
171 an *Nco*I site at the end of the 5'-UTR of *β2tubulin*. The 4272 bp ORF of Cas9 was then amplified
172 from pHsp70 Cas9 plasmid (Addgene plasmid #46294 (32)) using primers BR-34 and BR-35 and
173 inserted into the plasmid vector using *Nco*I and *Sal*I. Finally, the 3'-UTR fragment of *β2tubulin*
174 (AaegL5_2:326336649-326336454) was amplified using BR-28 and BR-29 and inserted into the
175 assembly plasmid vector using *Sal*I and *Xba*I. The entire cassette was then removable from
176 pUC19 using *Xho*I and *Xba*I for cloning into the TIMP-P4 or Carb109 destination vectors as either
177 *Xho*I/*Xba*I or *Xho*I/blunted insertions.

178

179 *Construction of the nanosCas9 cassette*

180 The 1159 bp *nanos* promoter fragment (AaegL5_1:228706-229865) was amplified from the HWE
181 strain of *Ae. aegypti* using primers BR-40 and BR-41 and cloned into pBluescript using *Xho*I
182 followed by screening for orientation using primers BR-99 and BR-41. The 4272 bp ORF of Cas9

183 was then amplified from the pHsp70 Cas9 plasmid (Addgene plasmid #46294 (32)) using primers
184 BR-34 and BR-35 and inserted into pBluescript downstream of the *nanos* promoter fragment
185 using a *Nco*I and *Sal*I digest for the PCR product and a *Pci*I/*Sal*I digest for the plasmid vector.
186 Finally, the 594 bp *nanos* 3'-UTR fragment (AaegL5_1:240330-240924) was amplified from the
187 *Ae. aegypti* genome (HWE strain) using primers BR-42 and BR-43 and cloned into the assembly
188 plasmid vector downstream of the Cas9 ORF using *Stu*I and *Nhe*I.

189

190 *Construction of Carb109-zpgCas9^{GD}*

191 The 1729 bp *zpg* promoter fragment (AaegL5_2:84862322-84863150) was amplified from
192 genomic DNA of the HWE strain of *Ae. aegypti* using primers BR-655 and BR-656. The promoter
193 region for the *zpg* gene in the HWE strain contained a 144 bp deletion (positions
194 AaegL5_2:84863229-848632372), which was 825 bp upstream of the +1 ATG of the *zpg* ORF.
195 The PCR product containing the promoter region was digested with *Xho*I and *Xba*I and cloned
196 into pBluescript. In addition, primer BR-655 was internally tagged with a *Bbs*I site to allow for
197 downstream scarless introduction of Cas9. The 1357 bp 3'-UTR of the *zpg* gene
198 (AaegL5_2:84865497-84866853) was amplified from *Ae. aegypti* (HWE strain) genomic DNA
199 using primers BR-660 and BR-683 and cloned into the vector containing the *zpg* promoter using
200 *Pst*I and *Spe*I. In addition, primer BR-660 was internally tagged with an inverted *Bbs*I site to
201 allow for downstream scarless introduction of Cas9. Subsequently, the 4272 bp ORF of Cas9 was
202 amplified from pHsp70 Cas9 plasmid (Addgene plasmid #46294 (32)) using primers BR-666 and
203 BR-667 and cloned into the vector between the *zpg* promoter and the 3'-UTR for *zpg* using *Bbs*I
204 for scarless, directional cloning.

205

206 *Assembly of the Carb109-3xP3-eCFP eye marker vector*

207 The Carb109-3xP3-eCFP vector was constructed by replacing the mCherry ORF from the Carb109
208 destination vector with eCFP. The eCFP ORF was amplified from plasmid AeaeCFPT4 using
209 primers BR-100 and BR-101 (17). The mCherry-deleted backbone from the empty Carb109
210 destination vector was amplified using BR-98 and BR-99. The two PCR fragments were then

211 assembled using the HiFi Gibson Assembly kit from NEB (Waltham, MA) following the
212 manufacturer's instructions.

213

214 *Assembly of the Pol-III promoter/chiRNA 'empty' vector*

215 The active U6 promoter from Konet *et al*., 2007 (33) was synthesized as a gBlock (IDT,
216 Corralville, IA) starting with the promoter region for AAEL017774 (AaegL5_3:382122755-
217 382123154, minus strand) with a G to A substitution at the -6 position relative to the TATA box
218 in order to domesticate a *Bbs*I restriction site and allow for Golden-Gate cloning (34). The sgRNA
219 scaffold from Dang *et al*. (2015) (35) was placed downstream of the promoter and separated by
220 two inverted *Bbs*I sites oriented such that the generated 5' overhang regions were present
221 within the promoter and chiRNA respectively (36). Primers tagged with *Sac*II restriction sites
222 were used to PCR amplify the full gBlock cDNA, which was then cloned into pBluescript using
223 *Sac*II. Subsequently, the sgRNA programming for all gRNA was prepared by digesting the empty
224 Pol III promoter/chiRNA vector with *Bbs*I followed by ligation of the respective adapter primers
225 (BR- 360 and BR-361 for the TIMP-P4 locus, BR-362 and BR-363 for the Carb109 locus). Adapters
226 were unphosphorylated and tagged with 5'-AAAT for the protospacer sequence (PAM-sense
227 strand) and 5'-AAAC for the corresponding reverse complement (PAM antisense strand),
228 following the approach outlined in Gokcezade *et al*., 2014 (36). The respective programmed U6-
229 sgRNA cassettes were then amplified using BR-350 and BR-351 and cloned into the destination
230 vectors using *Sac*II followed by screening for orientation using the appropriate forward adapter
231 (BR-360 for TIMP-P4 and BR-362 for Carb109) and M13R primers.

232

233 *Assembly of the pAeT7ku70 plasmid for dsRNA production*

234 A total of 10 fourth instar *Ae. aegypti* (HWE strain) larvae were collected, flash frozen on dry ice
235 and then extracted for total RNA using TRIzol reagent (Carlsbad, CA). First strand cDNA synthesis
236 was performed using the Protoscript cDNA kit (NEB, Waltham, MA) following the manufacturer's
237 instructions. The ku70 dsRNA template was then amplified from the cDNA using primers BR-44
238 and BR-45, which tagged both ends of the PCR product with the T7 promoter (37).

239 Subsequently, the T7-tagged PCR product was amplified using *Hind*III-tagged T7 (BR-80) and
240 cloned into pUC19 using *Hind*III.

241

242 *Final assemblies of GD constructs*

243 The final assemblies of the gene drive constructs were prepared using a three-step cloning
244 strategy. Cas9 cassettes for the TIMP-P4 or the Carb109 locus were cloned into their respective
245 destination vectors using *Xho*I/*Sac*II, followed by the addition of the mCherry fluorescent marker
246 under control of the 3xP3 synthetic promoter (38) using *Xho*I, and finally the addition of the
247 appropriate U6 promoter plus sgRNA using *Sac*II. The schematic for our GD constructs is
248 presented in **Figure S2**, and the primers used in our study are listed in **Table S5.** The final
249 sequences for the constructs are available at NCBI as outlined in **Table S6**.

250

251 **Generation of transgenic lines**

252 *Mosquito rearing*

253 The HWE strain of *Ae. aegypti* was used for the generation of all transgenic lines in our study.
254 The larval stages were reared in deionized water at 28°C with a 12:12 (L:D) photoperiod and fed
255 a diet of Tetramin Tropical flakes (Tetra Spectrum Brands Pet, LLC, Blacksburg, VA). Pupae were
256 transferred to plastic containers and allowed to emerge in 18 cubic-inch cages and provided
257 with deionized water and raisins as food sources.

258 *CRISPR/Cas9 target site identification*

259 For our initial testing, we first assessed the activities of six sgRNAs for activity proximal to the
260 Carb109 genome locus, while the active sgRNA for the TIMP-P4 genome locus was already
261 reported (17). To accomplish this, we prepared all injection mix material so that the final
262 concentrations of Cas9-NLS protein was 300 ng/µL and the concentration of sgRNA was 80
263 ng/µL. Then, three sets of approximately 100 pre-blastoderm embryos were injected with
264 injection mix and incubated overnight (18 h – 24 h) at 27°C before being homogenized and
265 extracted for gDNA into each of three pools. The genomic sequence of the Carb109 locus was

266 then PCR amplified using primers BR-60 and BR-65, and the resulting amplicons gel-purified
267 using the Zymo Clean and Concentrator kit (Zymo Research, San Diego, CA). PCR products were
268 subsequently sequenced at the University of Missouri Genomics Technology Core and analyzed
269 visually for trace decay at the predicted CRISPR/Cas9 cleavage site. All products were sequenced
270 in both directions to confirm the correct site of sequence decay.

271 *Harvest and microinjection of embryos*

272 Cages of 7-10 day-old mosquitoes were provided with a blood meal (defibrinated sheep blood,
273 Colorado Serum, Denver, CO) and maintained at 28°C under a 12:12 (L:D) photoperiod for four
274 days prior to injection. Groups of 15-20 hyper-gravid females were then mouth aspirated into an
275 aluminum foil-wrapped 50 mL conical tube containing two 2.5 x 0.5 cm strips of moistened,
276 overlapping Whatman #1 filter paper and allowed to oviposit for 20 min. Early embryos were
277 then aligned over a period of 20 to 30 min using a fine spotter paint brush such that all posterior
278 ends of the embryos faced the same direction. Aligned embryos were then transferred to
279 double-faced tape (Scotch brand, 3M Columbia, MO) affixed to a plastic coverslip (Fisher
280 Scientific, Waltham, MA) and covered with a layer of Halocarbon 27 oil (Sigma-Aldrich, St. Louis,
281 MO) prior to the visible onset of melanization. Embryos were then injected with injection mix
282 using a pulled and beveled micropipette capillary tube (Sutter Instruments, Novato, CA)
283 connected to a Femtojet 5247 air compressor (Eppendorf, Germany) at 650 psi positive pressure
284 and 100 psi backpressure. Immediately following injection, the Halocarbon 27 oil was gently
285 washed from the embryos with deionized water, and the embryos were allowed to age in a
286 humid chamber for a minimum of 2 h prior to transfer to a 500 mL plastic beaker lined with 5-10
287 layers of moistened Kimwipes. Injected embryos (herein referred to as G_0) were then
288 maintained in the humid plastic beaker for 6 days, transferred to a small plastic cup filled with
289 deionized water and allowed to hatch out. G_0 survivors were reared as described above and
290 backcrossed to non-transgenic HWE. For the backcrossing, male G_0 individuals were individually
291 provided with 5-10 virgin females and allowed to mate for 3-5 days then pooled into larger
292 cartons using 20 of the smaller cartons for each large carton. Female G_0 were collected into
293 large cartons (up to 100 per carton) and provided with half the number of virgin HWE males and
294 allowed to mate for 3-5 days. All cages were then provided with a minimum of three blood
295 meals (defibrinated sheep blood, Colorado Serum) and allowed to lay eggs onto filter papers. G_1

296 eggs were allowed to mature for five days and were then hatched, reared to fourth instar, and
297 screened for the presence of the fluorescence marker. Positive G_1 individuals were subsequently
298 outcrossed to HWE again to establish the transgenic lines. Integration of the transgene was
299 validated by PCR and Sanger sequencing using primers BR-13 and BR-115 for transgenes at the
300 Carb109 locus and primers BR-51 and BR-73 at the TIMP-P4 locus.

301

302 *Genetic crosses to test for GD activity*

303 An initial pool of G_0 hemizygous individuals was established for each of the gene drive lines by
304 outcrossing 40 transgenic males to 200 HWE virgins *en masse* and allowing them to mate and
305 take a blood meal. The G_0 eggs were subsequently collected and used as the starting material
306 for each of the drive activity crosses in our study. From the G_0 pools, a total of 12 hemizygous
307 males were individually crossed to two virgin HWE females, and 20-25 hemizygous females were
308 crossed to an equal number of male HWE *en masse* and allowed to mate for 3-5 days. The
309 individual "male founder" containers were each provided with their own blood meals, while the
310 "female founder" container was provided with a common blood meal, followed by the transfer
311 of blood-fed females to individual cartons for egg laying. Following oviposition, egg papers were
312 removed and allowed to develop for a minimum of five days prior to hatching individually into 4
313 oz plastic cups. Larvae were reared to third/fourth instar and scored for the presence of the
314 transgenic marker to determine the level of gene drive inheritance. Following the scoring of the
315 outcross-1 (OX-1) mosquitoes, two pools of crosses representing either a 'low' level (*i.e.*,
316 Mendelian-like), or 'high' level (*i.e.*, Super-Mendelian-like) were selected from each cross such
317 that an additional 12 female and 12 male G_1 hemizygotes could be outcrossed again to HWE for
318 the OX-2 assessment. The selection of the 'low' and 'high' pool, therefore, did not necessarily
319 represent the lowest and highest levels of gene drive inheritance, but rather served as
320 representative pools from which to establish the following outcross. From within OX-1, non-
321 transgenic individuals were saved to assess for the presence of GDBI. For the AeaNosC109^{GD} and
322 AeaZpgC109^{GD} lines, all non-transgenic mosquitoes were selected for assessment, while for the
323 AeaNosT4^{GD} and Aeaβ2tC109^{GD} lines, a total of 20 and 10 individuals were selected, respectively.
324 All crosses were duplicated and the data pooled for analysis.

325

326 *Statistical analyses*

327 Comparisons of the OX-1 gene drive levels for the lines were assessed in R using a Kruskal-
328 Wallace non- parametric ANOVA followed by a Dunn-Bonferroni *post hoc* means separation
329 procedure to test for significance across all groups and all lines. Comparisons of the OX-2 gene
330 drive levels, and assessments of gene drive blocking indels were conducted in R using a Kruskal-
331 Wallace nonparametric ANOVA followed by a Dunn-Bonferroni *post hoc* means separation
332 procedure to test for significance among individual crosses for all groups within each line.
333 Comparisons of the maternal and paternal contributions were assessed using pairwise T-testing
334 in R following a Shapiro-Wilk test for normality. Deviation from the expected Mendelian
335 inheritance level for the eCFP marker in the paternal contribution testing was conducted
336 manually using Chi-Square analysis.

337

338 *Testing of maternal contribution of Cas9-ribonucleo-protein (RNP)*

339 Initial crosses to establish trans-heterozygous mosquitoes were conducted using AeaNosC109^{GD}
340 females outcrossed to males harboring a 3xP3-eCFP-SV40 fluorescent eye marker at the
341 Carb109 locus (**Figure S3**). The positionings of the fluorescent markers in both transgenes were
342 in opposite orientation to one another to mitigate the potential for crossing over. Following this
343 cross, fourth instar progeny were screened and selected for the presence of both an mCherry
344 (gene drive) and an eCFP (null drive) marker. From this cross, 500 females of either the
345 AeaNosC109^{GD} or the AeaZpgC109^{GD} lines were outcrossed to 200 HWE males. Approximately
346 1000 embryos resulting from these crosses were then microinjected with 100 ng/µL of sgRNA
347 targeting the TIMP-P4 locus. Three rounds of injection, each > 1000 embryos were performed
348 for each of the crosses. Embryos were allowed to develop for one week prior to hatch, then
349 surviving larvae were reared to L3 and genotyped under a fluorescent microscope for the
350 presence of either the eCFP marker or mCherry marker. The DNA was then individually
351 extracted from each larva and assessed for GDBI at both the Carb109 and TIMP-P4 loci as
352 previously described.

353 With this assay, any activity at the Carb109 locus in the male (non-transgenic) allele for
354 AeaeCFPC109 mosquitoes would indicate a maternal provisioning of both the Cas9 and the
355 sgRNA targeting the Carb109 locus. Since it was possible that the Cas9 protein could be
356 inherited without the sgRNA, we further injected the early embryos with the sgRNA targeting
357 the TIMP-P4 locus. This allowed for us to interrogate whether Cas9 had been supplied
358 maternally (AeaeCFPC109 inheriting progeny) or if Cas9 had been supplied maternally and could
359 also be expressed in the early embryo/larva (mCherry GD inheriting).

360

361 *Testing of parental effect resulting in GD activity*

362 To test for a parental effect that results in GD activity, trans-heterozygous crosses were
363 performed as similarly described for the testing of the maternal effect, with the addition that
364 crosses were performed reciprocally to include male trans-heterozygous parentals as well. The
365 progeny from these crosses were scored for the numbers of offspring containing either mCherry
366 or an eCFP eye marker to test for the possibility of a fitness cost at the germline level relative to
367 the eCFP (null drive) marker. The female progeny from each of these crosses were saved (within
368 cross) and subsequently mated to an equal number of HWE males, then provided with a single
369 blood meal after which females were separated to allow them to lay eggs individually. Eggs were
370 allowed to mature for at least 5 d, then hatched and scored for the presence of the eCFP marker
371 to determine the level of transgene inheritance.

372

373 *Assessment of GDBI*

374 GDBI were assessed as inheritable refractory indels by analyzing the nucleotide sequence of the
375 alternative inheritable allele in outcrossed hemizygous individuals. For the OX-1 generation of
376 the gene drive assessment assays, non-transgenic mosquitoes were individually analyzed by PCR
377 using primers BR-20 and BR-23 for the TIMP-P4 locus and BR-60 and BR-65 for the Carb109
378 locus. PCR products were amplified, purified using the Zymo Clean and Concentrator kit (Zymo
379 Research, San Diego, CA), and Sanger sequenced. Chromatogram traces were then assessed
380 manually for trace decay at the predicted CRISPR/Cas9 cleavage site. For the assessment of GDBI

381 in the OX-2 generation, all non-transgenic mosquitoes within a cross were pooled and their DNA
382 extracted to obtain an 'average' number of GDBI for the non-drive-inheriting mosquitoes. PCR
383 products were then amplified using primers BR-724 and BR-725 for the Carb109 locus and BR-
384 726 and BR-727 for the TIMP-P4 locus to obtain the 'round 1' PCR products for Illumina whole-
385 amplicon sequencing. The first round PCR was held to 30 cycles. PCR products were
386 subsequently purified using the Zymo Gel Extraction kit (Zymo Research, San Diego, CA) and
387 adjusted to 1 ng/uL using a Qubit fluorimeter (ThermoFisher Scientific, Waltham MA), and
388 material was subsequently sequenced using paired end reads of 250 bp length (PE250) on an
389 Illumina MiSeq instrument. The resulting reads were trimmed using Cutadapt v1.01 (39) and
390 assessed for indels using Crispresso v2 (40). The output files of Crispresso v2 containing
391 insertions, deletions, and substitutions (assumed to be a composite event of deletion/insertion)
392 were then summed up to generate the value for 'indels'.

393

394 **Fitness cost studies**

395 Life parameter data was collected from male hemizygote AeaNosC109^{GD} and AeaZpgC109^{GD}
396 parentals as well as from HWE for comparison. Each fitness measurement was calculated as an
397 average from a minimum of 100 individual egg papers per mosquito strain $\pm$ standard error of
398 the mean. All data were analyzed with one-way ANOVA, and if a significant difference was
399 found, one-tailed t-tests were performed comparing HWE and each transgenic line. All
400 mosquitoes were maintained at 28 °C with 75 –80% relative humidity and a 12 h light / 12 h dark
401 cycle. Data are displayed in **Table S7**.

402

403 *Fecundity*

404 Three to five days post-emergence, hemizygous males or HWE males were mated *en masse* with
405 virgin HWE females in ratios of 5 males : 1 female using 64 oz. cartons (WebstaurantStore,
406 catalog number: 76 999SOUP64WB) each containing ~ 150 mosquitoes. Around 2-3 days later,
407 females were offered an artificial blood meal containing defibrinated sheep blood (Colorado
408 Serum Co., Denver, CO, USA) and 10 mM ATP, after which engorged females were retained. Two
409 to three days later, individual females were placed in 50 ml conical tubes lined with Whatman
410 Grade 1 Qualitative Filter Paper (catalog number: 1001-824) and filled with ~ 5 ml tap water.

411 Females were allowed to lay eggs for 1-2 days. Papers were visually inspected for eggs, which
412 were then quantified for fecundity, defined as the number of eggs a female oviposited in one
413 gonotrophic cycle. Egg papers were dried for a minimum of 5 days.
414
415 *Fertility, sex ratios, larva viability, and larva-to-pupa development*
416 Individual egg papers were hatched in ~ 100 ml freshly sterilized deionized water using ProPak
417 1600 polypropylene clear deli containers (Webstaurant) and were offered a ground fish food
418 (Tetramin, Melle, Germany) slurry *ad libitum*. Around 2-3 days post-initial hatch, the egg papers
419 were removed from the water and were allowed to dry again overnight. All egg papers were
420 then rehatched in the same containers from which they were initially hatched. Larvae (2nd-4th
421 instars) were visually inspected under a fluorescent microscope for expression of the mCherry
422 eye marker. Both positive and negative larvae were counted, but negative larvae were
423 eventually discarded. Fertility was calculated as the total number of larvae / total number of
424 eggs. Female and male pupae were collected every day, up to 14 days post-hatch, and the
425 timepoints of pupation were recorded. Around 150 mosquitoes (either males or females) of
426 each mosquito line were each pooled into small cups and allowed to emerge in 64 oz cartons.
427 Sex ratio was defined as the total number of males or females / the total number of pupae; larva
428 viability was defined as the total number of pupae / total number of eggs; and larva-to-pupa
429 development was defined as the average time to pupae development post-egg hatch.
430
431 *Male competition and adult longevity*
432 Using virgin adults, 50 transgenic and 50 HWE males (age matched) were allowed to mate with
433 100 HWE females for 2-3 days. Females were then offered an artificial blood meal containing
434 defibrinated sheep blood and 10 mM ATP. Eggs from individual engorged females were
435 obtained as described above for the fecundity assay. Around 5 days later, the egg papers were
436 hatched in sterile water, and larvae were fed ground Tetramin fish food *ad libitum*. Larvae (2nd-
437 4th instars) were visually inspected under a fluorescent microscope for the expression of the
438 mCherry eye marker. Male competition data was calculated as the number of positive G_2 larvae
439 / total number of larvae. For the longevity assay, 50 male and 50 female transgenic mosquitoes
440 (3-5 days post-emergence) were maintained in 64 oz. containers and offered raisins (as a sugar
441 source) and water. Every day, the number of dead mosquitoes was recorded and longevity was

442 calculated as the average number of days passed when 50% of the male or female mosquitoes
443 had died across cartons.
444
445 **MGDrivE population modeling**
446 The mosquito GD explorer (MGDrivE v 1.6.0) was used to model the inheritance of the
447 AeaNosC109^{GD} and AeaZpgC109^{GD} lines (41). A stable population was set to 10000 mosquitoes
448 at a 1:1 sex ratio with no migration out of, or into, the main patch. A single release of 2000
449 homozygous male mosquitoes (20%) was simulated at day 25 for 100 stochastic samplings for
450 1500 days (AeaNosC109^{GD}) and 4000 days (AeaZpgC109^{GD}). In the MGDrivE package, the cube
451 "Cube-CRISPR2MF.R" allows for sex-specific rates of drive and allows for the modeling of two
452 types of resistance alleles: those that block the GD, yet cause no fitness cost (R), and those that
453 block the GD but result in a fitness cost (B). Since it was predicted that a GDBI occurring in an
454 intergenic locus would cause no fitness cost, we modified the tMatrices in the cube script
455 "Cube-CRISPR2MF.R" to still allow for sex-specific rates of drive and indel causing activities, but
456 we condensed the (R) and (B) alleles to a common (R) allele, which represented all GDBI and
457 assumed no fitness cost to that genotype. The modified gtype and tMatrices are provided as
458 **Table S8**. We further plotted an additional figure panel that summed females with any
459 combination of genotypes containing a GD allele and any combination of genotypes without a
460 GD allele to simulation. These values were used to estimate the proportion of a hypothetical
461 linked antiviral effector gene to represent females having a viral refractory phenotype. The
462 parameters used for our model and how they were calculated are provided in **Table S9**. The
463 entomological parameters popGrowth and muAD were left as default, based on literature. tEgg
464 and tPupa were assumed to be 5 and 2, respectively, based on standard laboratory rearing
465 practices and observations. tLarva was calculated as the average number of days of larva-to-
466 pupa development. betaK was calculated as the average fecundity * 4 (the average number of
467 blood meals a female takes during her lifetime) / 11 (the average lifespan of a female mosquito
468 in an urban environment) (42). They were determined from **Table 3** by adding the marker
469 positive mosquitoes from the "low" and "high" pools together to obtain the total number of
470 correct homing events. The number of incorrect homing events (*i.e.*, GDBI formation) was
471 estimated by multiplying the total number of marker-negative mosquitoes from the "low" and
472 "high" pools by the fraction of the tested OX-1 marker-negative progeny identified to contain

473 GDBI. This was done in place of a direct count since some of the samples from the OX-1 marker-
474 negative larvae did not provide a PCR product that could be sequenced for the assessment of
475 GDBIs. Then, to calculate the parameters cF and cM, the number of marker positive and GDBI
476 positive mosquitoes were summed and divided by the total N. From this number, the proportion
477 that gave rise to correct homing events was determined as chF and chM, with the resistance
478 rate formation parameters crF and crM calculated as 1-chF or 1-chM, respectively. The rate of
479 maternal deposition, dF, was calculated as the average rate of GDBI observed for the Carb109
480 locus for eCFP-inheriting offspring from the trans-heterozygous cross between the GD and the
481 eCFP-blocked GD. For both the AeaNosC109^{GD} and AeaZpgC109^{GD} line, we then further set the
482 rate of correct maternal effect homing (dhF) to 0 and the rate of incorrect maternal effect
483 homing (drF) to 1. Larval viability was significantly reduced for the AeaNosC109^{GD} line, which we
484 incorporated into the model under the xiF/xiM variables by subtracting the average larval
485 viability of the HWE strain from the average larval viability of the AeaNosC109^{GD} line. In the
486 AeaZpgC109^{GD} line, the larval viability was slightly higher than in HWE, but not significantly
487 different. Therefore, we set the parameters xiF and xiM to NULL for the AeaZpgC109^{GD} line.
488 Finally, since Li *et al*. (2020) similarly found that their transgenic split GD had an overall fitness
489 similar to the parental Liverpool strain, yet still included a 10% fitness cost for their modeling,
490 we incorporated an overall decrease in fertility by 10% for both of our modeled GD lines (10).

491

492 **RESULTS**

493 *Identification of active target sites and target site polymorphisms*

494 Prior to testing the GD lines, we first identified two targets for CRISPR/Cas9 cleavage, which
495 were located in non-protein encoding regions of the mosquito genome. In our previous work
496 (17), we identified a highly active sgRNA for the TIMP-P4 locus (**Table 1**). In our current work, we
497 identified a novel active CRISPR/Cas9 target site for the Carb109 locus located 1214 bp
498 downstream of the *mariner/Mos1* insertion site, which is the defining locus in the DENV2-
499 resistant Carb109 line (13). Since the Carb109 *mariner/Mos1* insertion was determined to be
500 within the 3'-UTR of the polyadenylate-binding protein gene (AAEL010318), we manually
501 selected CRISPR/Cas9 targets as close to, but not within, the AAEL010318 gene locus and

502 assessed for off-targets using CHOPCHOP v2 (43). In total, we assessed six sgRNA for activity
503 (**Table 1**) and identified only a single sgRNA (#15) that showed DNA cleavage activity. Therefore,
504 for all CRISPR/Cas9 based experiments at the Carb109 locus, sgRNA #15 was selected. While
505 sgRNA #15 was ideal for our GD testing in the laboratory-adapted HWE strain of *Ae. aegypti*, we
506 further wanted to estimate how conserved the sgRNA #15 target was in field strains of this
507 mosquito species. In addition to the assessment of sgRNA activity, we therefore also analyzed
508 both genomic target sites, TIMP-P4 and Carb109, for polymorphisms using data from Schmidt *et*
509 *al* (2020), which examined CRISPR/Cas9 target sites across 132 genomes of *Ae. aegypti* (44). Two
510 polymorphisms were found in the TIMP-P4 locus: one in the protospacer adjacent motif (PAM)
511 that changed the second base G to a T and had an allele frequency of 0.026 among the 132
512 genomes tested, while the second polymorphism was at position 13 distal to the PAM that
513 changed the base from a G to a C at an allelic frequency of 0.009 (**Table S1**). The Carb109 locus
514 contained only a single polymorphism at position 19 distal to the PAM that still allows for the
515 use of an 18 bp protospacer, which is considered functional for Cas9 activity (45). Although most
516 of the data from Schmidt et al (2020) is derived from *Ae. aegypti* populations in California, we
517 assumed no polymorphisms for the TIMP-P4 and Carb109 loci in regard to our population
518 modeling.

519

520 *Establishment of transgenic Ae. aegypti lines*

521 A total of six transgenic lines were established via homologous recombination with embryo
522 injection efforts ranging from 568 – 1442 embryos (**Table 2**). In general, the survival rate of the
523 injected G_0 mosquitoes ranged from a low of 3.9% (AeaeCFPC109) to a high of 23%
524 (AeaNosC109^{GD}). In addition, we found that the *nanos*Cas9-U6sgRNA constructs required no
525 helper Cas9 or helper sgRNA to integrate into the genome. Due to the timing of expression of
526 native *nanos*, there was co-expression of Cas9 from the injected plasmid, and due to the
527 ubiquitous expression of the AAEL017774 U6 gene, there was co-expression of sgRNA as well.
528 Regardless, after the initial successful injection of the *nanos*Cas9-U6sgRNA construct into the
529 TIMP-P4 locus, helper Cas9 protein was added to all injection mixes, with the omission of the
530 helper sgRNA and continued inclusion of the ku70 dsRNA trigger.

531

532 *GD inheritance rates over two outcrossed generations*

533 To test for the rates of GD inheritance, a starting population was established by outcrossing
534 transgenic males to non-transgenic HWE females to establish hemizygous "OX-0" (outcross 0)
535 mosquitoes. This was performed to ensure that all mosquitoes used for testing were
536 hemizygous. Overall, the strongest GD performance was observed in the AeaNosC109^{GD} line,
537 where the median inheritance rate among progeny was 70% and 73% for male and female
538 parentals, respectively (**Figure 1**; **Table S2**). Further, the levels of drive ranged from no drive, 45-
539 48%, (comparable to Mendelian inheritance rates) to super-Mendelian rates, reaching up to
540 96% (**Figure 1; Table S2**). When the same cargo was inserted and retargeted for the TIMP-P4
541 locus, however, no GD activity was observed with median values for marker inheritance
542 remaining at 48% and 46% for male and female parentals, respectively (**Figure 1**; **Table S2**).
543 Taken together, these results show that *nanos*Cas9 GDs were principally functional in *Ae.*
544 *aegypti* and overall GD activity was strongly influenced by the GD's genomic insertion site.
545 Regarding the *β2tubulin*Cas9 controlled GD construct, the median values for marker inheritance
546 demonstrated no drive activity for the Aeaβ2tC109^{GD} line, with overall transgene inheritance
547 rates resembling Mendelian inheritance patterns as they ranged from a low of 43% in male
548 parentals (n = 24/56) to a high of 55% in both male (n = 16/29) and female (n = 11/20) parental
549 groups. Given that GD activity was observed at the Carb109 locus using the *nanos* promoter, we
550 tested another promoter in the same locus, *zero population growth (zpg)*, which has been
551 shown to have strong GD activity in *An. gambiae* but has not yet been tested in *Ae. aegypti* (46,
552 47). The median GD inheritance rates for the AeaZpgC109^{GD} line were 56% and 68% for male
553 and female parentals, respectively (**Figure 1**; **Table S2**). The male transgenic parentals had a
554 significantly lower (p = 0.0258) level of drive when compared to either parental cross for the
555 AeaNosC109^{GD} line, or to female transgenic parentals of the AeaZpgC109^{GD} line. These results
556 showed that while the *zpg* promoter is active in *Ae. aegypti*, there may be a sex-specific effect
557 on Cas9 expression, which was not anticipated for this promoter since the *zpg* gene (*innexin-4*)
558 is involved in early germ cell development in both male and female *Drosophila* (48). Further,
559 given that the median GD inheritance rates for the Aeaβ2tC109^{GD} line were below 50% for both
560 male and female parentals, it suggested that there was no CRISPR/Cas9 activity in the germline

561 for this line. Recent work by Terradas *et al* (2021) indicated that in *An. gambiae*, the *β2-tubulin*
562 promoter is expressed post-meiotically, which could explain why we did not see GD activity
563 when using this promoter (49). Therefore, we did not continue the Aeaβ2tC109^{GD} line for further
564 assessment at the OX-2 level. Meanwhile, although the AeaNosT4^{GD} line also did not
565 demonstrate any GD activity, its cargo was identical to that of the AeaNosC109^{GD} line,
566 prompting us to continue this line for further assessment at the OX-2 level.

567 Regarding the OX-2 crosses, we were interested in answering two questions: 1) Would the
568 effects of 'low' and 'high' levels of GD inheritance from the OX-1 crosses be consistent? and 2)
569 Do GD blocking indels (GDBI) accrue differently for female and male transgenic parentals? We
570 assessed for these by first identifying individual crosses from each of the OX-1 groups that
571 represented 'low' and 'high' levels of drive (**Table 3**), and subsequently outcrossed transgenic
572 female and males reciprocally to HWE mosquitoes as was performed in OX-1. This resulted in a
573 total of eight crossing groups within each line to which we applied three-letter codes that
574 identified the parental (F 'female' or M 'male'), the grandparental (F 'female' or M 'male'), and
575 the level of drive observed for the OX-1 pool (L 'low' or H 'high'). When the progeny (n ranging
576 from 795 to 3162) for all OX-2 crosses were scored, we again observed Mendelian-like
577 inheritance of the GD cassette for the AeaNosT4^{GD} line. However, one cross in the FFH group
578 resulted in 90% inheritance (n = 124), suggesting that while GD activity was inefficient at the
579 TIMP-P4 locus, occasional cases of drive might still occur (**Figure 2; Table S3**). The results for the
580 AeaZpgC109^{GD} line displayed similar levels of drive for all 157 crosses, with median inheritance
581 rates ranging from 50% in the MML group to 60% in the FMH group (**Figure 2; Table S3**).
582 Further, among all AeaZpgC109^{GD} crosses, five groups contained individual crosses that
583 demonstrated > 80% rate of GD inheritance (**Figure 2**; **Table S3**). These results suggest that the
584 effect of 'low' or 'high' level of drive was not inheritable by the OX-2 generation. Finally, for the
585 AeaNosC109^{GD} line, the median GD inheritance rates ranged from a low of 56% in the FML group
586 to a high of 77% in the MFL group (**Figure 2; Table S3**). Of particular interest was that in the
587 AeaNosC109^{GD} line, there were outcrosses that occasionally resulted in 100% inheritance of the
588 GD. While these events were rare, they were found across multiple parental and grandparental
589 groups, including the MMH, MFH, FFL, and MFL groups (n = 20, 44, 114, and 137, respectively)
590 (**Figure 2; Table S3**). These results highlight that while, overall, the crossing groups within line

591 AeaNosC109^{GD} line displayed GD inheritance rates ranging from 57% to 76% (**Table S3**),
592 complete drive (100% inheritance) was achievable. Given that the levels of GD in the
593 AeaNosC109^{GD} line were statistically similar ($p > 0.05$) for male parentals with any grandparental
594 combinations irrespective of their 'low' or 'high' level of GD origins, we ruled out the effect of
595 grandparent sex and the possibility that the trait of 'low' or 'high' GD levels was inheritable.

596

597 *Accrual of GD blocking indels (GDBI)*

598 To better understand why a broad range in GD activity was observed, we assessed for the
599 occurrence of GDBI among the OX-1 and OX-2 crosses. Overall, the occurrence of GDBI in the
600 OX-1 crosses was most pronounced in the AeaNosC109^{GD} line, which also demonstrated the
601 highest average level of GD (**Figures 1,2**; **Table 3**). Meanwhile, the *zpg* promoter similarly
602 displayed some GDBI, albeit at a much lower level (7.4% for 'low' GD individuals, and 4.3% for
603 'high' GD individuals), and only in pools of offspring originating from females. For both the
604 Aeaβ2tC109^{GD} and AeaNosT4^{GD} lines, no GDBI were identified in the OX-1 crosses; however,
605 these lines did not demonstrate GD activity and had Mendelian-like inheritance of the marker;
606 thus, it was not expected that GDBI would arise in these lines as there was likely no CRISPR/Cas9
607 activity. Given that the GDBI identified in the OX-1 crosses were inherited from the original
608 transgenic males, which had been crossed to HWE females in the OX-0 cross, we further
609 assessed the levels of GDBI for the OX-2 crosses to identify any differences between female and
610 male groups with respect to the number of GDBI that arose in the population (**Figure 3; Table**
611 **S4**). Overall, we identified negligible proportions (< 5%) of amplicons containing GDBI in the
612 AeaNosT4^{GD} line, comparable to the single HWE control sample (**Figure 3**). This observation was
613 in accordance with the results of the OX-1 GDBI assessment, and again was likely due to the lack
614 of activity of CRISPR/Cas9 when the GD was positioned at the TIMP-P4 locus. Regarding the
615 assessment of the OX-2 GDBI in the AeaNosC109^{GD} line, all crossing groups displayed variable
616 proportions of amplicons containing GDBIs. In addition, we observed nine crosses for which the
617 proportion of amplicons containing GDBI was 50%. A proportion of 50% represents the
618 theoretical maximal proportion of amplicons that can contain indels when considering
619 outcrossed (GD-negative) larvae. Of these nine crosses, two data points were close to 50% (FFL:

620 54%, MFL: 53%), while the remaining seven data points ranged from 64% (MMH) to 100%
621 (MML). These elevated proportions of amplicons containing r GDBI could be an artifact of PCR
622 chimera. Thus, our analysis of pooled larvae based on high-throughput sequencing was likely
623 overestimating the actual number of GDBI in the sample. One crossing group within the
624 AeaNosC109^{GD} line, MFH, contained very few amplicons showing the presence of indels (median
625 = 14.5%); however, the median proportion of amplicons containing indels was not significantly
626 lower in this group than in the other crossing groups within the AeaNosC109^{GD} line (p = 0.0831).
627 Finally, in the AeaZpgC109^{GD} line, a significantly greater median number of GDBI was observed
628 for the FFL group (median = 2.6%) when compared to the MMH (median = 0.02%) group. In
629 general, all male parental crosses appeared to have fewer GDBI (median range = 0.02% - 1.6%)
630 than the female parental crosses (median range = 2.0% - 11.9%), regardless of the sex of the
631 grandparental transgenic individual. As explained above, this result was unexpected for the *zpg*
632 promoter (48). Interestingly, there was no apparent grandparental effect for the *zpg*Cas9
633 controlled GD. In addition to the abundance of GDBI assessed for the OX-2 cross, we also
634 assessed the size distributions of the resultant insertions/deletions (**Figure S1**). Overall,
635 deletions were the most abundant type of indel, representing 86%, 94%, and 97% of all indels
636 for the AeaNosT4^{GD}, AeaNosC109^{GD}, and AeaZpgC109^{GD} lines, respectively. Nearly all identified
637 deletions were present within 50 bp of the CRISPR/Cas9 target site, with the largest deletion
638 being 82 bp in the AeaZpgC109^{GD} line. The largest identified insertion was 60 bp in the
639 AeaNosC109^{GD} line, although nearly 100% of the insertions in all lines tested were within 50 bp
640 of the CRISPR/Cas9 target site. Taken together, these results suggest that for the purpose of an
641 autonomous GD system in *Ae. aegypti*, the homologous region required for strand invasion of
642 the cleaved DNA proximal to the predicted CRISPR/Cas9 target is likely a minimum of 50 bp in
643 size.

644

645 *Testing for maternal contribution of CRISPR/Cas9*

646 Maternal and/or paternal contribution of the CRISPR/Cas9 components leads to extra-germline
647 activity of the Cas9 ribonucleo-protein (RNP) in the early embryo, which could result in the
648 development of GDBI. Notably, this will occur in offspring that do not inherit the GD allele,

649 which in the absence of a donor for HDR would cause GDBI formation. To test for maternal
650 contribution, the paternal allele must be distinctly identifiable from the inherited maternal allele
651 when the GD allele is absent. Previous studies have used recessive phenotypes to identify these
652 effects (10, 50-51), where the maternal allele is balanced over a null-allele for the recessive
653 marker and the female is then outcrossed to a wildtype male. The progeny from this cross is
654 phenotypically wildtype and genotypically heterozygous. In the event of cleavage of the paternal
655 allele, however, the progeny will be biallelic/homozygous and display the recessive phenotype.
656 Since we targeted an intergenic locus, we accomplished the same goal through the development
657 of the AeaeCFPC109 line, which contained a marker-only cargo and no GD construct: a
658 codominant alternate color marker (eCFP). This construct was then integrated into the *Ae.*
659 *aegypti* genome through homologous recombination using sgRNA #15 and was therefore
660 positioned at the same (Carb109) locus as the mCherry-marked GD systems. Since the sgRNA
661 #15 target site was interrupted by the 3xP3-eCFP marker, it established a "blocked drive"
662 because the sgRNA #15 protospacer is no longer present in the genome. When the
663 AeaeCFPC109 line is crossed to either the AeaNosC109^{GD} or the AeaZpgC109^{GD} lines, offspring
664 containing both eCFP and mCherry eye markers would harbor one allele with an eCFP marker,
665 and the other allele with the mCherry-marked GD. No drive or GDBI activity would occur in the
666 germline as the genomic GD target is blocked by the eCFP marker meaning that the
667 Carb109/sgRNA #15 locus is no longer present (**Figure S3**). The genotypes of the eggs of trans-
668 heterozygous females resulting from the cross will then consist of either the mCherry-marked
669 GD or the GD blocking eCFP marker. When these trans-heterozygous females are outcrossed to
670 non-transgenic male HWE mosquitoes, the males will contribute an allele that is targetable by
671 CRISPR/Cas9 in the embryo. This then can allow for GD/cleavage activity to be assessed. Given
672 that CRISPR/Cas9 activity requires both the Cas9 protein and the sgRNA transcript, we further
673 microinjected embryos from the cross with synthetic sgRNA targeting a secondary genomic
674 locus (TIMP-P4 locus). These assays allowed us to reveal any maternal effect in the early embryo
675 and this way provided insight to possible early embryo (extra-germline) activity of CRISPR/Cas9
676 components. Three sets of approximately 1000 embryos were injected for each of the HWE
677 outcrossed trans-heterozygotes (WT X [AeaNosC109^{GD}/ AeaeCFPC109], and WT X
678 [AeaZpgC109^{GD} /AeaeCFPC109]) and allowed to develop to third instar to enable visual
679 genotyping of the fluorescent marker (**Table 4**). DNA was extracted from individually surviving

680 mosquitoes and PCR followed by Sanger sequencing was conducted across both the Carb109
681 and TIMP-P4 loci to assess for the presence of GDBI at the target loci. We observed for both the
682 AeaNosC109^{GD} and the AeaZpgC109^{GD} lines CRISPR/Cas9 activity in the GD-targeted Carb109
683 locus and in the TIMP-P4 locus targeted via injected sgRNA. We also found that the survival rate
684 of sgRNA-injected trans-heterozygotes was lower when compared to that of the sgRNA injected
685 (non-transgenic) HWE strain, which could be due to the concurrent targeting of two loci on
686 different chromosomes.
687
688 In general, the CRISPR/Cas9 activity observed for maternal deposition (inheriting the eCFP eye
689 marker) was highest in the AeaNosC109^{GD} line, with 40% of the larvae demonstrating Cas9
690 activity at the TIMP-P4 locus and 19% displaying Cas9 activity at the Carb109 GD locus (**Figure**
691 **4**). In the AeaZpgC109^{GD} line, 16% and 13% of larvae exhibited Cas9 activity at the TIMP-P4 and
692 Carb109 sites, respectively, although statistically, these values were not significantly different
693 across genomic targets or mosquito lines ($p > 0.05$) (**Figure 4**). We did, however, find that in the
694 AeaNosC109^{GD} line, significantly more indels were detectable at the Carb109 locus when the GD
695 allele was inherited ($p = 0.0309$). In addition, there were significantly more indels present among
696 GD inheriting progeny from the AeaNosC109^{GD} line than among GD inheriting progeny arising
697 from the AeaZpgC109^{GD} line crosses ($p = 0.0051$). Taken together, these results suggest a clear
698 and strong maternal inheritance of the CRISPR/Cas9 RNP. Furthermore, early embryonic activity
699 of Cas9 was stronger when additional sgRNA was supplied, either exogenously through
700 microinjection of synthetic TIMP-P4 targeting sgRNA, or endogenously as Pol-III expressed
701 sgRNA in the GD inheriting larvae.

702

703 *Testing for a parental contribution of CRISPR/Cas9 resulting in GD activity*

704 To test for a parental effect resulting in GD activity, we performed reciprocal trans-heterozygous
705 crosses as outlined above. In addition to female trans-heterozygotes outcrossed to non-
706 transgenic males, we also tested male trans-heterozygotes outcrossed to non-transgenic
707 females. In the first outcross (OX-1) of the trans-heterozygotes individuals, we found that the
708 inheritance rates of the eCFP eye marker and the mCherry-marked GD were nearly 50% for both

709 females and males (**Figure 5**) and were not statistically different when tested using pairwise T-
710 testing (p = 0.5911 and p = 0.7587, respectively). When females from the eCFP-inheriting
711 individuals were further outcrossed to non-transgenic (OX-2) to investigate the level of parental
712 GD contribution, the median inheritance rate was 47% for offspring from eCFP expressing
713 females and 49% for offspring from eCFP expressing male parentals, providing no evidence for a
714 parental effect resulting in GD activity; regardless, a few data points were greater than 50% with
715 two points reaching ~80% (**Figure 5**).

716

717 *Fitness of GD harboring mosquitoes and modeling of GD performance over multiple generations*

718 Based on the experimentally derived data regarding GD inheritance including frequency of GDBI
719 accrual, testing for maternal effect of the CRISPR/Cas9 RNP, and analysis of fitness parameters
720 of the GD harboring mosquito lines (**Table S7**), we modeled the performance of AaeNosC109^{GD}
721 or AeaZpgC109^{GD} in a hypothetical field release scenario for the purpose of population
722 replacement (**Figure 6; Table S8, Table S9**). To model the lines, we used the MGDrivE mosquito
723 population modeling package in R (41) and modeled for a static population of *Ae. aegypti* with a
724 stable population size of 10,000 mosquitoes at a sex ratio of 1:1. We allowed for a single release
725 of males at day 25 at a rate of 1/5th of the population (*i.e.*, 2000 homozygous male mosquitoes)
726 and ran 100 stochastic simulations for each of the transgenic lines until the allelic frequencies of
727 the genotypes stabilized. Given that we targeted an intergenic region, all GBDI were assumed to
728 incur no fitness cost to the mosquito, and we therefore merged the 'B' allele from MGDrivE (*i.e.,*
729 a GD resistance allele that results in a fitness cost) with the 'R' allele (GD resistance allele with
730 no fitness cost), such that all resistance alleles had the same fitness as the non-transgenic alleles
731 (**Table S8**). **Figure 6** displays the various prevalence levels of each genotype in the predicted
732 model for females (all genotypes), males (all genotypes), and females divided between
733 genotypes carrying at least one copy of the GD (displayed as "Hypothetical antiviral effector
734 gene" to model a linked antiviral effector) and genotypes not carrying the GD (displayed as
735 "Wildtype"). Overall, there was a rapid decline in the number of wildtype mosquitoes for both
736 simulated releases and the rate at which the genotypes stabilized within a population differed
737 between the two transgenic lines. In the AeaNosC109^{GD} line, the homozygous wildtype genotype
738 was eliminated by ~400 days-post release (PR) in the simulated closed system, with the

739 hemizygous GD (no GDBI) and homozygous GD genotypes quickly replacing the homozygous
740 wildtype genotype. By 450-500 days PR, however, the GDBI harboring resistance allele genotype
741 became dominant and rapidly overtook the population eventually causing the GD to fall out of
742 the population and the near entirety of the population to contain GDBI alleles by 1500 days PR.
743 When a hypothetical antiviral effector linked to the GD was considered, the proportion of
744 female mosquitoes carrying at least one copy of the antiviral effector gene peaked at 320 to 370
745 days PR with ~80% of females carrying at least one copy of the antiviral effector. Any window of
746 antiviral protection soon closed, and the GD was eliminated from the population by 1500 days
747 PR. By comparison, the AeaZpgC109^{GD} line also eliminated the homozygous wildtype genotype
748 by ~400 days PR while GDBI resistance alleles became the dominant genotype in the population
749 by ~1000 days PR. Although the AeaZpgC109^{GD} was found to have lower GD inheritance rates
750 than AeaNosC109^{GD}, it was able to drive at least one copy of the GD through the population,
751 reaching > 95% among all female mosquitoes by ~420 days PR. Similar to the AeaNosC109^{GD} line,
752 the window of protection for the hypothetically linked antiviral effector eventually closed due to
753 the fitness differences between the GD and the GD-resistant (GDBI) alleles (**Table S9**), with >
754 50% of females losing the antiviral effector by ~1500 days PR.

755

756 **DISCUSSION**

757 Previous GD studies in mosquitoes have targeted recessive marker genes that provide for a
758 visual phenotype when both alleles are disrupted. Since we selected intergenic loci, TIMP-P4
759 and Carb109, any disruption of these loci would not result in recessive phenotypes. We
760 therefore positioned a codominant marker at the Carb109 locus, which then allowed us to
761 distinguish between the GD cassette (mCherry marked) and a blocked drive (marked by eCFP).
762 The CRISPR/Cas9 RNP requires two components: the Cas9 protein, and the sgRNA transcript.
763 The Cas9 endonuclease was placed under control of a maternally-provisioned gene promoter,
764 *nanos*, in the AeaNosC109^{GD} line or the germline-essential promoter for *innexin4* (*zpg*) in the
765 AeaZpgC109^{GD} line (47, 52-53). Earlier work by Akbari *et al* (2013) indicated that both *nanos* and
766 *innexin4* transcripts were detectable in the early embryo for up to 48 h, suggesting that *innexin4*
767 (*zpg*) could be maternally-provisioned, a finding that was further supported based on

768 observations from *zpg* knock-out studies in *Drosophila* (48, 54). In addition to Cas9, the active
769 CRISPR/Cas9 RNP requires a sgRNA to guide the Cas9 protein for DNA cleavage. In our study, the
770 expression of the sgRNA was under control of a snoRNA Pol-III promoter, which allowed for
771 multiple possibilities of maternal inheritance of the CRISPR/Cas9 system. Assuming that Cas9
772 was maternally provisioned as either protein or mRNA, the possibilities of maternal inheritance
773 included: 1) inheritance of the full Cas9-RNP complex, 2) inheritance of the Cas9 mRNA and
774 sgRNA transcripts, 3) inheritance of Cas9 mRNA and/or protein, but not the sgRNA transcript. To
775 test for this, we independently crossed the AeaNosC109^{GD} and AeaZpgC109^{GD} lines to the
776 AeaeCFPC109 line to create females which, when mated to wildtype males, would have progeny
777 that either inherited the GD or the null (non-editable) allele at the Carb109 locus.

778 The spatio-temporal expression of transgenes in *Ae. aegypti* is strongly influenced by the
779 promoter used for expression as well as the genomic transgene insertion site, which can be
780 affected by position effect variegation (55, 56). The importance of genomic position for optimal
781 Cas9 activity in *Ae. aegypti* was identified in the work by Li *et al*. (2017), where the activity of
782 Cas9 expression varied by genomic locus when placed under control of six different promoters
783 and integrated into the *Ae. aegypti* genome in a quasi-random fashion using the *piggyBac*
784 transposable element (29). The forward approach from Li *et al*. (2017) allowed for the
785 identification of optimal genomic insertion loci for Cas9 activity in the germline, while in our
786 study, we took a reverse approach by utilizing two genomic loci (TIMP-P4 and Carb109)
787 previously identified to be highly permissive to antiviral transgene expression (13, 17). Our
788 reasoning for this was that if the GD cassettes were positioned in a genomic locus that
789 supported a strong expression of antiviral effectors, the entire system could be built and
790 established as a single-component autonomous GD line. It was unclear, how an autonomous GD
791 in an intergenic locus would perform. Our reverse engineering approach demonstrated that
792 genomic loci that are well-suited towards the expression of antiviral effectors may not
793 necessarily be ideal for the functioning of a CRISPR/Cas9 autonomous GD system. Notably, the
794 presence of the GD system at the TIMP-P4 locus resulted in no GD activity and further
795 demonstrated a very low level of inheritable GDBI when assessed via whole-amplicon
796 sequencing. This suggests that the GD components were not efficiently expressed in the
797 germline when positioned at the TIMP-P4 locus although our previous work demonstrated

798 strong expression of transgenes in the adult female midgut at the same locus (17, 31).
799 Meanwhile, a second genomic locus that had also been shown to be ideal for stable antiviral
800 activity (*i.e.*, Carb109; [13]) exhibited high GD activity; however, there was a concomitant level
801 of GDBI detectable that eventually blocked the GD in a population modeling simulation. This
802 demonstrated that while the Carb109 locus supported GD activity by allowing rapid
803 introgression of either GD cassette into the target population, the locus was prone to the
804 generation of heritable GDBI, which over time blocked and eliminated the GD in the population
805 modeling. These results suggest that when an autonomous CRISPR/Cas9 based GD is positioned
806 at an intergenic locus, it will likely be self-exhausting. Our simulation models provided valuable
807 information regarding the dynamics of the GD. For example, the AeaZpgC109^{GD} line provided a
808 wider hypothetical window of protection (females harboring at least one copy of the GD and a
809 hypothetical antiviral effector) than the AeaNosC109^{GD} line, although the latter GD line had
810 stronger GD inheritance. The major differences in GD performance and biological parameters
811 between the AeaNosC109^{GD} and AeaZpgC109^{GD} lines were the levels of GD activity, female
812 deposition rate, resistance allele formation rate, and pupation success. To estimate which of
813 these effects most strongly influenced the performance of the GD, we conducted simulations of
814 the AeaNosC109^{GD} line in which maternal deposition rate, resistance allele formation rates, or
815 pupation success parameters were substituted with the respective (experimentally determined)
816 parameters from the AeaZpgC109^{GD} line (**Figure S4**). However, there was no appreciable
817 difference in overall GD persistence when the levels of GDBI resistance alleles, or the levels of
818 maternal deposition were reduced in the AeaNosC109$^{GD\text{-}SIMULATED}$ line to those of the
819 experimental AeaZpgC109^{GD} line (**Figure S4**). When the parameter of pupation success was
820 modified to match that of the AeaZpgC109^{GD} line, the GD and associated hypothetical antiviral
821 effector persisted through the population with approximately half of the females carrying at
822 least one copy of the transgene up to ~3000 days PR. These simulations suggest that while the
823 rates of GD inheritance, GDBI resistance allele formation, and maternal deposition were
824 important factors, it was the fitness of the GD line that had the greatest impact on the dynamics
825 of GD inheritance. A study by Terradas *et al* (2021) investigated the deposition of germline
826 expressed genes in the developing oocytes of autonomous *Anopheles* sp. GD lines (49), including
827 the AgNosCd1^{GD} line (23, 49), which used the *nanos* promoter and 3'UTR for Cas9 expression. In
828 their study, the authors found that *nanos* driven Cas9 transcripts were indeed expressed in the

829 nurse cells along with native *nanos* transcripts; however, unlike the native *nanos* transcripts, the
830 Cas9 transcripts were found at very low levels or were even absent in the developing oocyte
831 (49). In males, by contrast, Cas9 expression controlled by the *nanos* regulatory elements
832 paralleled that of the native *nanos* transcript. In regard to the *β2-tubulin* regulatory elements, it
833 was shown by the same authors that in *An. stephensi, β2-tubulin* transcripts were male-specific.
834 In addition, transcript expression occurred in the late stages of spermatogenesis, which may not
835 be a suitable time window of expression when attempting to use the *β2-tubulin* promoter for a
836 CRISPR/Cas9 based GD. Indeed, this could be a reason for the lack of GD activity that we
837 observed for our Aeaβ2tC109^{GD} line. Furthermore, Terradas *et al* (2021) investigated the pattern
838 of native *zpg* expression and found that its expression pattern was similar to that of *vasa* but at
839 a lower general level. They found that there was expression of *zpg* throughout premeiotic and
840 meiotic stages in males and high-level *zpg* expression in the sperm flagella, which could increase
841 the prevalence of GDBI. In our AeaZpgC109^{GD} line, however, we identified a lower level of GDBI
842 for male parentals and a lower level of GD compared to the AeaNosC109^{GD} line. Thus, it is likely
843 that the expression of the Cas9 transcript under control of the *zpg* promoter does not perfectly
844 parallel that of the native *zpg* transcript. Furthermore, although the *An. gambiae* AgNosCd1^{GD}
845 line did not have an appreciable deposition of mRNA transcripts for Cas9 when expressed from
846 the *nanos* promoter and 3'UTR (49), a recent analysis of GDBI by Carballar-Lejarazú *et al* (2022)
847 found that there was indeed a maternal effect of CRISPR/Cas9 activity in the AgNosCd1^{GD} line
848 (50). Taken together, these results suggest that the maternal contribution could be provisioned
849 to the developing oocyte as residual Cas9 RNP complex might be expressed during early
850 germline development and further persist in the zygote.

851 Simulations of the different GD performances and life parameters of the AeaNosC109^{GD} and
852 AeaZpgC109^{GD} lines highlight the importance of fitness and maternal contribution with respect
853 to the accrual of GDBI. Our population modeling revealed that in the absence of any fitness
854 costs directly associated with GDBI, yet there was still a fitness cost associated with the GD as
855 such because an autonomous GD in an intergenic locus will ultimately block itself due to the
856 accrual of GDBI alleles and the drive will be lost. Therefore, an accumulation of GDBI alleles will
857 ultimately exhaust and impair the GD. Given the significance of these observations obtained
858 from our simulated release study, multi-generational cage trials aiming at modeling population

859 replacement under more realistic field conditions (22, 23) will be imperative in the future to
860 confirm the effects of fitness cost on single-component GD performance in *Ae. aegypti*.

861 Since we selected intergenic loci, which were assumed to have no effect on fitness if cleaved,
862 the persistence of the autonomous drive system could be strengthened by its placement into a
863 non-neutral (*e.g.*, coding region) locus as performed for *kh* in *An. stephensi* (21, 22). This could
864 also extend the window of protection provided by the antiviral effector. There are
865 environmental concerns regarding the release of transgenes into wild mosquito populations,
866 and furthermore, there is a practical rationale for a non-persistent GD: the associated
867 antipathogen effector gene could lose its efficacy over time. Such a loss of efficacy could be due
868 to adaptations of the pathogen to evade the effect of the antipathogen effector gene, or
869 spontaneous mutations leading to a loss of function of the antipathogen effector. An
870 autonomous GD system that will ultimately self-block may have several benefits as it could
871 rapidly drive an antipathogen transgene through wild mosquito populations while providing a
872 window of protection from a circulating arbovirus, before dropping out of the population due to
873 the fixation of GDBI alleles.

874

875 **DATA AVAILABILITY**

876

877 The nucleotide sequences for all our GD constructs listed in Table S6 are available at NCBI
878 (ncbi.nlm.nih.gov) under the following accession numbers. Construct AeaeCFPT4: accession #
879 MT926371; construct AeaeCFPC109: accession # OL452018; construct AeaNosT4GD: accession #
880 OL452014; construct Aeaβ2tC109GD: accession # OL452017; construct AeaNosC109GD:
881 accession # OL452015; construct AeaZpgC109GD: accession # OL452016; construct pAeU6-MT:
882 accession # OL452019; pAeT7ku70dsRNA: accession #: OL452021. The code modification to
883 MGDrivE is provided in Table S8. Supplementary material is available at G3 online.

884

885 **ACKNOWLEDGEMENTS**

886 We would like to thank Drs. Héctor Sánchez Castellanos, Rodrigo Corder, and John Marshall for
887 their guidance and assistance with the use of the MGDrivE simulation for population modeling.
888 We thank Drs. Hanno Schmidt and Gregory Lanzaro for kindly sharing the genomic vcf data for

889 the *Ae. aegypti* genomes. Thanks to Susi Bennett for all her mosquito maintenance. We also
890 thank the University of Missouri Genomics Technology Core for technical support.

891

892 **FUNDING**

893 The authors acknowledge the National Institutes of Health - National Institute of Allergy and
894 Infectious Diseases (NIH-NIAID) for the funding of this research work (grant applications: R01
895 AI130085-01A1, K.E.O and R56 AI167980-01, A.W.E.F.).

896

897 **CONFLICTS OF INTEREST**

898 None declared.

899

900 **AUTHOR CONTRIBUTIONS**

901 W.R., A.E.W., K.E.O., and A.W.E.F. designed research; W.R., A.E.W., J.L., I.S-V., and R.J.
902 performed research; W.R. contributed new reagents/analytic tools; W.R., A.E.W., K.E.O., and
903 A.W.E.F. analyzed data; and W.R., A.E.W., K.E.O., and A.W.E.F. wrote the paper.

904

905 **REFERENCES**

906 1. Weaver SC, Vasilakis N. 2009. Molecular evolution of dengue viruses: contributions of
907 phylogenetics to understanding the history and epidemiology of the preeminent arboviral
908 disease. Infect Genet Evol. 9(4):523-540.

909 2. Weaver SC, Reisen WK. 2010. Present and future arboviral threats. Antiviral Res. 85(2):328-
910 345.

911 3. Liu-Helmersson J, Brännström Å, Sewe MO, Semenza JC, Rocklöv J. 2019. Estimating Past,
912 Present, and 700 Future Trends in the Global Distribution and Abundance of the Arbovirus
913 Vector *Aedes aegypti* Under Climate Change Scenarios. Front Public Health. 7:148.

914 4. Manjarres-Suarez A, Olivero-Verbel J. 2013. Chemical control of *Aedes aegypti*: a historical
915 perspective. Rev. costarric. salud pública [online]. 2013, vol.22, n.1 68-75. Available from:

916 <http://www.scielo.sa.cr/scielo.php?script=sci_arttext&pid=S1409-
917 14292013000100012&lng=en&nrm=iso>. ISSN 1409-1429.

918 5. Liu N. 2015. Insecticide Resistance in Mosquitoes: Impact, Mechanisms, and Research
919 Directions. Annu Rev Entomol. 60:537–559.

920 6. Kittayapong P, Ninphanomchai S, Limohpasmanee W, Chansang C, Chansang U,
921 Mongkalangoon P. 2019. Combined sterile insect technique and incompatible insect technique:
922 The first proof-of-concept to suppress *Aedes aegypti* vector populations in semi-rural settings in
923 Thailand. PLoS Negl Trop Dis. 13(10):e0007771.

924 7. Beebe NW, Pagendam D, Trewin BJ, Boomer A, Bradford M, Ford A, Liddington C, Bondarenco
925 A, De Barro PJ, Gilchrist J, Paton C, Staunton KM, Johnson B, Maynard AJ, Devine GJ, Hugo LE,
926 Rasic G, Cook H, Massaro P, Snoad N, Crawford JE, White BJ, Xi Z, Ritchie SA. 2021. Releasing
927 incompatible males drives strong suppression across populations of wild and *Wolbachia* -
928 carrying *Aedes aegypti* in Australia. Proc Natl Acad Sci USA. 118(41):e2106828118.

929 8. Carvalho DO, McKemey AR, Garziera L, Lacroix R, Donnelly CA, Alphey L, Malavasi A, Capurro
930 ML. 2015. Suppression of a Field Population of Aedes aegypti in Brazil by Sustained Release of
931 Transgenic Male Mosquitoes. PLOS Negl Trop Dis 9(7):
932 e0003864. DOI:10.1371/journal.pntd.0003864.

933 9. Waltz E. 2021. First genetically modified mosquitoes released in the United States. Nature.
934 593:175-176.

935 10. Li M, Yang T, Kandul NP, Bui M, Gamez S, Raban R, Bennett J, Sánchez C HM, Lanzaro GC,
936 Schmidt H, Lee Y, Marshall JM, Akbari OS. 2020. Development of a confinable gene drive system
937 in the human disease vector *Aedes aegypti*. eLife. 9:e51701.

938 11. Li M, Yang T, Bui M, Gamez S, Wise T, Kandul NP, Liu J, Alcantara L, Lee H, Edula JR, Raban R,
939 Zhan Y, Wang Y, DeBeaubien N, Chen J, Sánchez C HM, Bennett JB, Antoshechkin I, Montell C,
940 Marshall JM, Akbari OS. 2021. Suppressing mosquito populations with precision guided sterile
941 males. Nat Commun. 12:5374.

942 12. Franz AW, Sanchez-Vargas I, Adelman ZN, Blair CD, Beaty BJ, James AA, Olson KE. 2006.
943 Engineering RNA interference-based resistance to dengue virus type 2 in genetically modified
944 *Aedes aegypti*. Proc Natl Acad Sci USA. 103(11):4198-4203.

945 13. Franz AWE, Sanchez-Vargas I, Raban RR, Black WC IV, James AA, Olson KE. 2014. Fitness
946 Impact and Stability of a Transgene Conferring Resistance to Dengue-2 Virus following
947 Introgression into a Genetically Diverse *Aedes aegypti* Strain. PLoS Negl Trop Dis. 8(5):e2833.

948 14. Yen PS, James AA, Li JC, Chen CH, Failloux AB. 2018. Synthetic miRNAs induce dual arboviral-
949 resistance phenotypes in the vector mosquito *Aedes aegypti*. Commun Biol. 1:11.

950 15. Buchman A, Gamez S, Li M, Antoshechkin I, Li H-H, Wang H-W, Chen C-H, Klein MJ,
951 Duchemin J-B, Paradkar PN, Akbari OS. 2019. Engineered resistance to Zika virus in transgenic

952 *Aedes aegypti* expressing a polycistronic cluster of synthetic small RNAs. Proc Natl Acad Sci USA.
953 116(9):3656-3661.

954 16. Buchman A, Gamez S, Li M, Antoshechkin I, Li HH, Wang HW, Chen CH, Klein MJ, Duchemin
955 JB, Crowe JE Jr, Paradkar PN, Akbari OS (2020) Broad dengue neutralization in mosquitoes
956 expressing an engineered antibody. PLoS Pathog. 16(1):e1008103.

957 17. Williams AE, Sanchez-Vargas I, Reid WR, Lin J, Franz AWE, Olson KE. 2020. The antiviral
958 small-interfering RNA pathway induces Zika virus resistance in transgenic *Aedes aegypti*. Viruses.
959 12(11):1231.

960 18. Burt A. 2003. Site-specific selfish genes as tools for the control and genetic engineering of
961 natural populations. Proc Biol Sci. 270(1518):921-928.

962 19. Windbichler N, Papathanos PA, Catteruccia F, Ranson H, Burt A, Crisanti A. 2007. Homing
963 endonuclease mediated gene targeting in *Anopheles gambiae* cells and embryos. Nucleic Acids
964 Res. 35(17):5922-5933.

965 20. Gantz VM, Bier E. 2015. The mutagenic chain reaction: A method for converting
966 heterozygous to homozygous mutations. Science. 348(6233):442-444.

967 21. Gantz VM, Jasinskiene N, Tatarenkova O, Fazekas A, Macias VM, Bier E, James AA. 2015.
968 Highly efficient Cas9-mediated gene drive for population modification of the malaria vector
969 mosquito Anopheles stephensi. Proc Natl Acad Sci USA. 112(49):E6736-E6743.

970 22. Adolfi A, Gantz VM, Jasinskiene N, Lee H-F, Hwang K, Terradas G, Bulger EA, Ramaiah A,
971 Bennett JB, Emerson JJ, Marshall JM, Bier E, James AA. 2020. Efficient population modification
972 gene-drive rescue system in the malaria mosquito *Anopheles stephensi*. Nat Commun. 11, 5553.

973 23. Carballar-Lejarazú R, Ogaugwu C, Tushar T, Kelsey A, Pham TB, Murphy J, Schmidt H, Lee Y,
974 Lanzaro GC, James AA. 2020. Next-generation gene drive for population modification of the
975 malaria vector mosquito, *Anopheles gambiae*. Proc Natl Acad Sci USA. 117(37):22805-22814.

976 24. Verkuijl SAN, Gonzalez E, Li M, Ang J, Kandul NP, Anderson MAE, Akbari OS, Bonsall MB,
977 Alphey L. 2020. A CRISPR endonuclease gene drive reveals two distinct mechanisms of
978 inheritance bias. bioRxiv 2020.12.15.421271. doi: 10.1101/2020.12.15.421271.

979 25. Wu, B., L. Luo, and X. J. Gao. 2016. Cas9-triggered chain ablation of Cas9 as a gene drive. Nat.
980 Biotechnol. 34:137–138.

981 26. Gantz, VM, Bier E. 2016. The dawn of active genetics. Bioessays. 38:50–63.

982 27. Chae K, Dawson C, Valentin C, Contreras B, Zapletal J, Myles KM, Adelman ZN. 2022.
983 Engineering a self-eliminating transgene in the yellow fever mosquito, *Aedes aegypti*, PNAS
984 Nexus. 2022:pgac037.

985 28. Zapletal J, Najmitabrizi N, Erraguntla M, Lawley MA, Myles KM, Adelman ZN. 2021. Making
986 gene drive biodegradable. Phil Trans R Soc B. 376:20190804.

987 29. Li M, Bui M, Yang T, Bowman CS, White BJ, Akbari OS. 2017. Germline Cas9 expression yields
988 highly efficient genome engineering in a major worldwide disease vector, *Aedes aegypti*. Proc
989 Natl Acad Sci USA. 114(49):E10540-E10549.

990 30. Williams AE, Franz AWE, Reid WR, Olson KE. 2020. Antiviral Effectors and Gene Drive for
991 Mosquito Population Suppression or Replacement to Mitigate Arbovirus Transmission by *Aedes*
992 *aegypti*. Insects. 11(1):52.

993 31. Dong S, Balaraman V, Kantor AM, Lin J, Grant DG, Held NL, Franz AWE. 2017. Chikungunya
994 virus dissemination from the midgut of *Aedes aegypti* is associated with temporal basal lamina
995 degradation during bloodmeal digestion. PLOS Negl Trop Dis. 11(9):e0005976.

996 32. Gratz SJ, Cummings AM, Nguyen JN, Hamm DC, Donohue LK, Harrison MM, Wildonger J,
997 O'Connor-Giles KM. 2013. Genome engineering of Drosophila with the CRISPR RNA-guided Cas9
998 nuclease. Genetics. 194(4):1029-1035.

999 33. Konet DS, Anderson J, Piper J, Akkina R, Suchman E, Carlson J. 2007. Short-hairpin RNA
1000 expressed from polymerase III promoters mediates RNA interference in mosquito cells. Insect
1001 Mol Biol. 16(2):199-206.

1002 34. Engler C, Kandzia R, Marillonnet S. 2008. A one pot, one step, precision cloning method with
1003 high-throughput capability. PLoS ONE 3(11):e3647.

1004 35. Dang Y, Jia G, Choi J, Ma H, Anaya E, Ye C, Shankar P, Wu H. 2015. Optimizing sgRNA
1005 structure to improve CRISPR-Cas9 knockout efficiency. Genome Biol. 16:280.

1006 36. Gokcezade J, Sienski G, Duchek P. 2014. Efficient CRISPR/Cas9 plasmids for rapid and
1007 versatile genome editing in *Drosophila*. G3 (Bethesda). 4(11):2279-2282.

1008 37. Basu S, Aryan S, Overcash JM, Samuel GH, Anderson MAE, Dahlem TJ, Myles KM, Adelman
1009 ZN. 2015. Silencing of end-joining repair for efficient site-specific gene insertion after
1010 TALEN/CRISPR mutagenesis in Aedes aegypti. Proc Natl Acad Sci USA. 112(13):4038-4043.

1011 38. Horn C, Jaunich B, Wimmer EA. 2000. Highly sensitive, fluorescent transformation marker for
1012 *Drosophila* transgenesis. Dev Genes Evol. 210(12):623--629.

1013 39. Martin M. 2011. Cutadapt removes adapter sequences from high-throughput sequencing
1014 reads. EMBnet.journal, 17(1):10-12.

1015 40. Clement K, Rees H, Canver MC, Gehrke JM, Farouni R, Hsu JY, Cole MA, Liu DR, Joung K,
1016 Bauer DE, Pinello L. 2019. CRISPResso2 provides accurate and rapid genome editing sequence
1017 analysis. Nat Biotechnol. 37:224–226.

1018 41. Sánchez C HM, Wu SL, Bennett, JB, Marshall, JM. 2020. MGDrivE: A modular simulation
1019 framework for the spread of gene drives through spatially explicit mosquito populations.
1020 Methods Ecol Evol. 11:229–239.

1021 42. Otero M, Solari HG, Schweigmann N.2006. A stochastic population dynamics model for
1022 *Aedes aegypti*: formulation and application to a city with temperate climate. Bull Math Biol.
1023 68(8):1945-1974.

1024 43. Labun K, Montague TG, Gagnon JA, Thyme SB, Valen E.2016. CHOPCHOP v2: a web tool for
1025 the next generation of CRISPR genome engineering. Nucleic Acids Res. 8;44(W1):W272-276.

1026 44. Schmidt H, Collier TC, Hanemaaijer MJ, Houston PD, Lee Y, Lanzaro GC. 2020. Abundance of
1027 conserved CRISPR-Cas9 target sites within the highly polymorphic genomes of *Anopheles* and
1028 *Aedes* mosquitoes. Nat Commun. 11:1425.

1029 45. Cencic R, Miura H, Malina A, Robert F, Ethier S, Schmeing TM, Dostie J, Pelletier J. 2014.
1030 Protospacer adjacent motif (PAM)-distal sequences engage CRISPR Cas9 DNA target cleavage.
1031 PLoS One. 9(10):e109213.

1032 46. Hammond A, Galizi R, Kyrou K, Simoni A, Siniscalchi C, Katsanos D, Gribble M, Baker D,
1033 Marois E, Russell S, Burt A, Windbichler N, Crisanti A, Nolan T. 2016. A CRISPR-Cas9 gene drive
1034 system targeting female reproduction in the malaria mosquito vector *Anopheles gambiae*. Nat
1035 Biotechnol. 34(1):78-83.

1036 47. Kyrou K, Hammond AM, Galizi R, Kranjc N, Burt A, Beaghton AK, Nolan T, Cristani A. 2018. A
1037 CRISPR—Cas9 gene drive targeting doublesex causes complete population suppression in caged
1038 *Anopheles gambiae* mosquitoes. Nat Biotech. 36:1062–1066.

1039 48. Tazuke SI, Schulz C, Gilboa L, Fogarty M, Mahowald AP, Guichet A, Ephrussi A, Wood CG,
1040 Lehmann R, Fuller MT. 2002. A germline-specific gap junction protein required for survival of
1041 differentiating early germ cells. Development. 129(10):2529-2539.

1042 49. Terradas G, Hermann A, James AA, McGinnis W, Bier E. 2021. High-resolution in situ analysis
1043 of Cas9 germline transcript distributions in gene-drive *Anopheles* mosquitoes. G3
1044 (Bethesda). 12(1):jkab369.

1045 50. Carballar-Lejarazú R, Tushar T, Pham TB, James AA. 2022. Cas9-mediated maternal effect
1046 and derived resistance alleles in a gene-drive strain of the African malaria vector mosquito,
1047 *Anopheles gambiae*. Genetics. 7:iyac055.

1048 51. Chaverra-Rodriguez D, Macias VM, Hughes GL, Pujhari S, Suzuki Y, Peterson DR, Kim D,
1049 McKeand S, Rasgon JL. 2018. Targeted delivery of CRISPR-Cas9 ribonucleoprotein into arthropod
1050 ovaries for heritable germline gene editing. Nat Commun. 9:3008.

1051 52. Adelman ZN, Jasinskiene N, Onal S, Juhn J, Ashikyan A, Salampessy M, MacCauley T, James
1052 AA. 2007. Nanos gene control DNA mediates developmentally regulated transposition in the
1053 yellow fever mosquito *Aedes aegypti*. Proc Natl Acad Sci USA. 104(24):9970-9975.

1054 53. Calvo E, Walter M, Adelman ZN, Jimenez A, Onal S, Marinotti O, James AA. 2005. *Nanos* (*nos*)
1055 genes of the vector mosquitoes, *Anopheles gambiae*, *Anopheles stephensi* and *Aedes aegypti*.
1056 Insect Biochem Mol Biol. 35(7):789-798.

1057 54. Akbari OS, Antoshechkin I, Amrhein H, Williams B, Diloreto R, Sandler J, Hay BA. 2013. The
1058 developmental transcriptome of the mosquito *Aedes aegypti*, an invasive species and major
1059 arbovirus vector. G3 (Bethesda) 3(9):1493-1509.

1060 55. Franz AW, Sanchez-Vargas I, Piper J, Smith MR, Khoo CC, James AA, Olson KE. 2009. Stability
1061 and loss of a virus resistance phenotype over time in transgenic mosquitoes harbouring an
1062 antiviral effector gene. Insect Mol Biol. 18(5):661-672.

1063 56. Henikoff S. 1992. Position effect and related phenomena. Curr Opin Genet Dev. 2(6):907-
1064 912.

1065

1066

1067

1068

1069

1070

1071

1072

1073

1074

1075

1076

1077

1078

1079

1080

1081

1082

1083

1084 **FIGURES**

1085

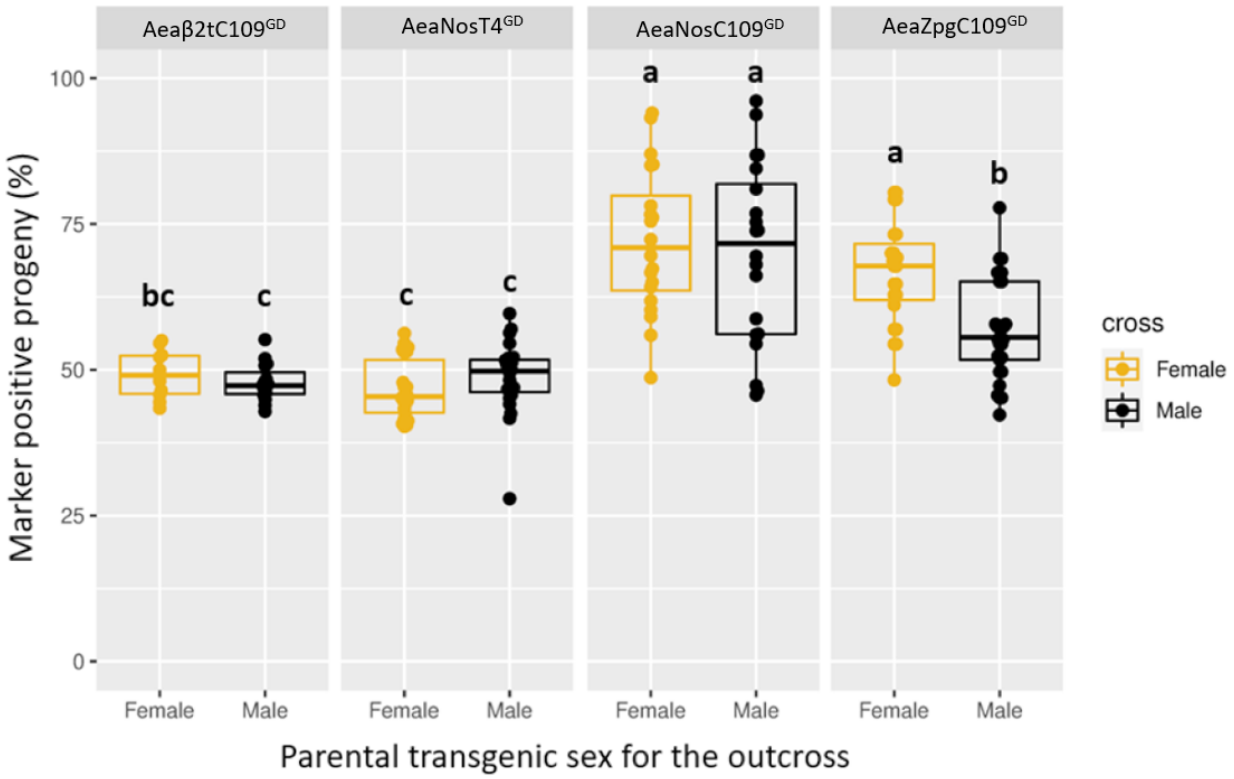

1086

1087

1088 **Figure 1. Frequency of marker gene inheritance in first-outcrossed (OX-1) individuals**
1089 **originating from hemizygous outcrossed females or males of transgenic lines harboring**
1090 **CRISPR/Cas9 based GDs at two different genomic loci (Carb109 and TIMP-P4) with Cas9**
1091 **expression under control of three different promoters (β*2tubulin*, *nanos*, or *zpg*).** The bar
1092 inside each box plot represents the median value, while the lower and upper borders of each
1093 box represent Q1 and Q3, respectively. Groups superseded with the same letter are not
1094 statistically different ($p > 0.05$). Each data point represents the percentage of transgene
1095 inheritance resulting from the offspring of the parental crosses where each transgenic female
1096 parental was allowed to mate with two non-transgenic males, and each transgenic male
1097 parental was allowed to mate with two non-transgenic females. A minimum of 20 larvae was set
1098 for each group in order to be scored. For the female parental crosses, the population sizes of
1099 each data point ranged from 20 to 142 larvae (mean ± SEM = 59 ± 3 larvae). For the male
1100 parental crosses, the population sizes of each data point ranged from 21 to 415 larvae (mean ±
1101 SEM = 91 ± 5 larvae).

1102

1103

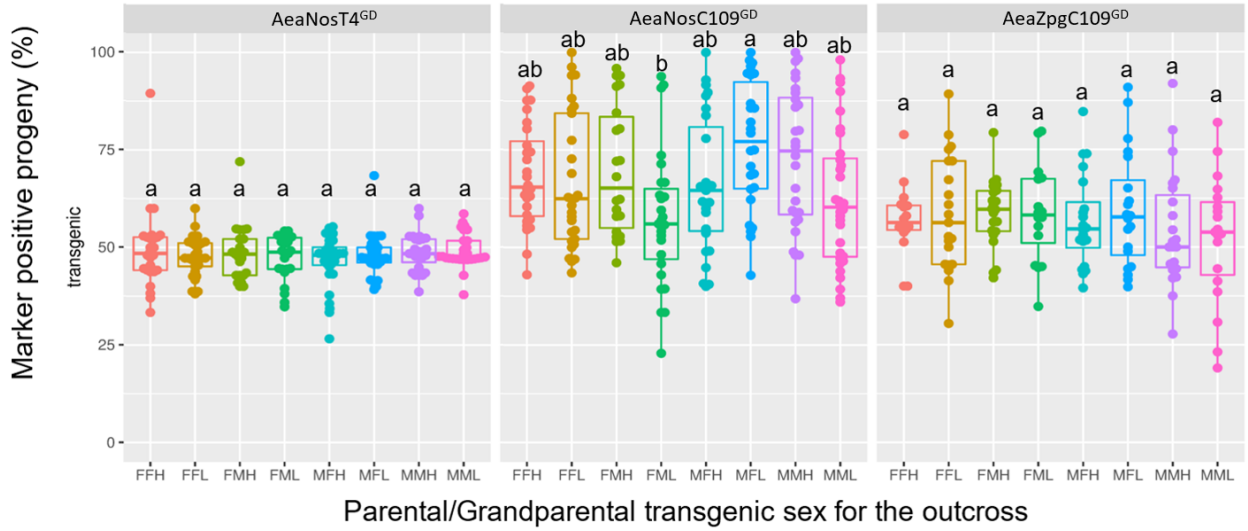

Figure 2. Frequency of marker gene inheritance in progeny from second-outcrossed (OX-2) individuals (594 groups, average n = 72 ± 2, total n = 43,015) originating from either 'high' or 'low' parental GD pools harboring the GD at two different genomic loci (Carb109 and TIMP-P4) with Cas9 expression under control of two different promoters (*nanos* or *zpg*). The bar inside each box plot represents the median value, while the lower and upper borders of the boxes represent Q1 and Q3, respectively. Groups within a GD line that are superseded with the same letter are not statistically different ($p > 0.05$). The first letter of each cross designation indicates the OX-2 parental transgenic sex and the second letter indicates the OX-1 grandparental transgenic sex, where F=female and M=male. L=Low/no drive level in the grandparental generation, H=high drive level in the grandparental generation. Each data point represents the percentage of transgene inheritance resulting from the offspring of the parental crosses where each transgenic female parental was allowed to mate with two non-transgenic males, and each transgenic male parental was allowed to mate with two non-transgenic females. A minimum of 20 larvae was set for each group in order to be scored.

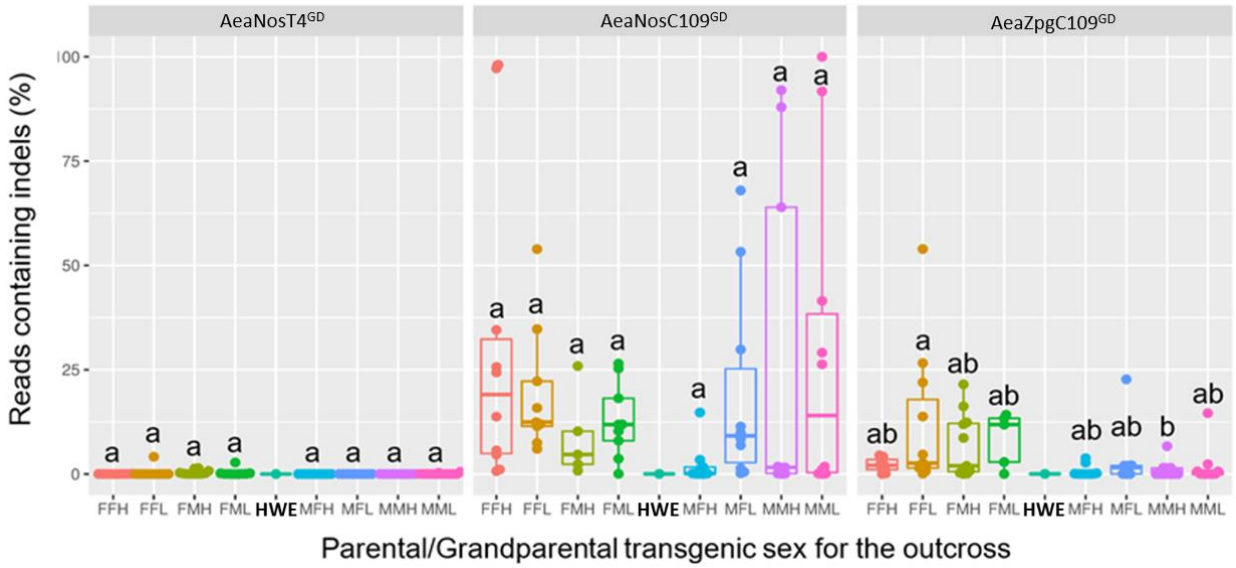

Figure 3. Proportions of PCR amplicons containing GDBI for pooled non-transgenic mosquitoes from the second-outcrossed (OX-2) GD lines originating from either 'high' or 'low' parental GD pools harboring the GD at two different genomic loci (Carb109 or TIMP-P4) and Cas9 expression under control of two different promoters (*nanos* or *zpg*). The bar inside the box plot represents the median value, while the lower and upper borders of the boxes represent Q1 and Q3, respectively. Indels were analyzed via high-throughput nucleotide sequencing. The first letter within each cross indicates the parental transgenic (OX-2) sex, the second letter indicates the grandparental (OX-1) transgenic sex. L=Low/no drive level in the parental generation, H=High drive in the parental generation. HWE=Higgs' white eye non-transgenic. Each data point represents the percentage of high-throughput reads containing a GDBI obtained from PCR amplicons that spanned the genomic target site for either Carb109 or TIMP-P4 locus. The gDNA template used for each PCR reaction consisted of the pooled contribution of all non-transgenic larvae from the OX-2 crosses.

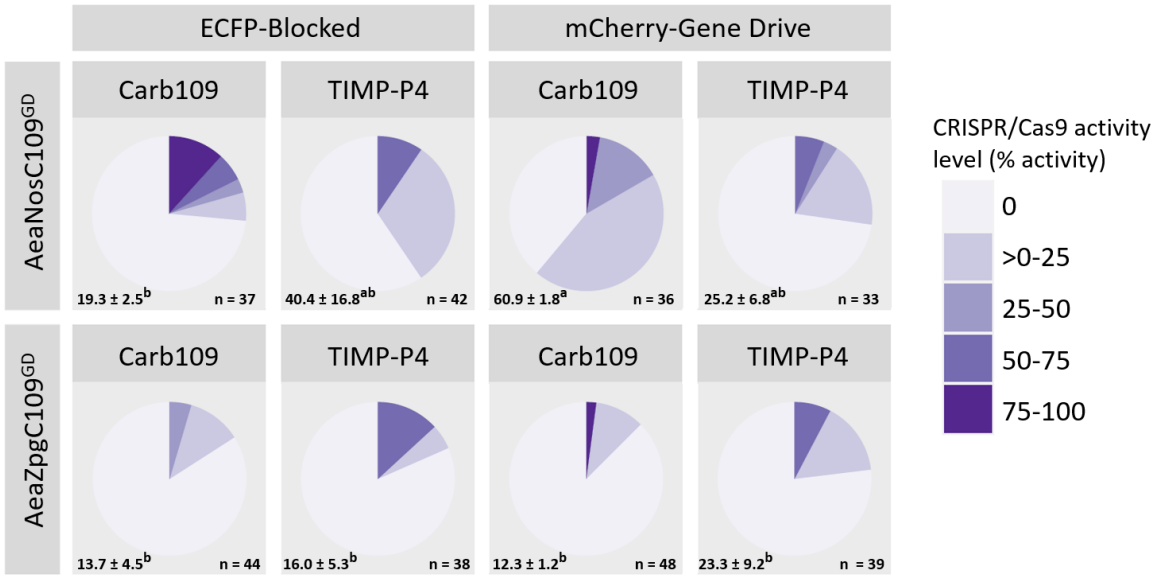

Figure 4. Maternal contributions of CRISPR/Cas9 components in the AeaNosC109^{GD} and AeaZpgC109^{GD} lines. GD lines (marked with mCherry) were balanced against a blocked GD (marked with eCFP) present at the CRISPR/Cas9 target site, and female trans-heterozygotes were then outcrossed to non-transgenic males. Average numbers of larvae +/- SEM and mean grouping are indicated for each group in the lower left-hand corner. Average and SEM superscripted with the same letter are not significantly different ($p > 0.05$). Total numbers of assessed larvae across all three replicates are indicated in the lower right corner. The embryos from this cross were subsequently injected with sgRNA targeting the TIMP-P4 locus, and the surviving larvae were reared to third instar, genotyped, and assayed for CRISPR/Cas9 activity at both the Carb109 locus (GD target) and the TIMP-P4 locus (exogenously applied sgRNA) via PCR and Sanger sequence trace analysis. The estimates of CRISPR/Cas9 activity were made using the Synthego ICE tool, which compares an edited trace to a non-transgenic trace.

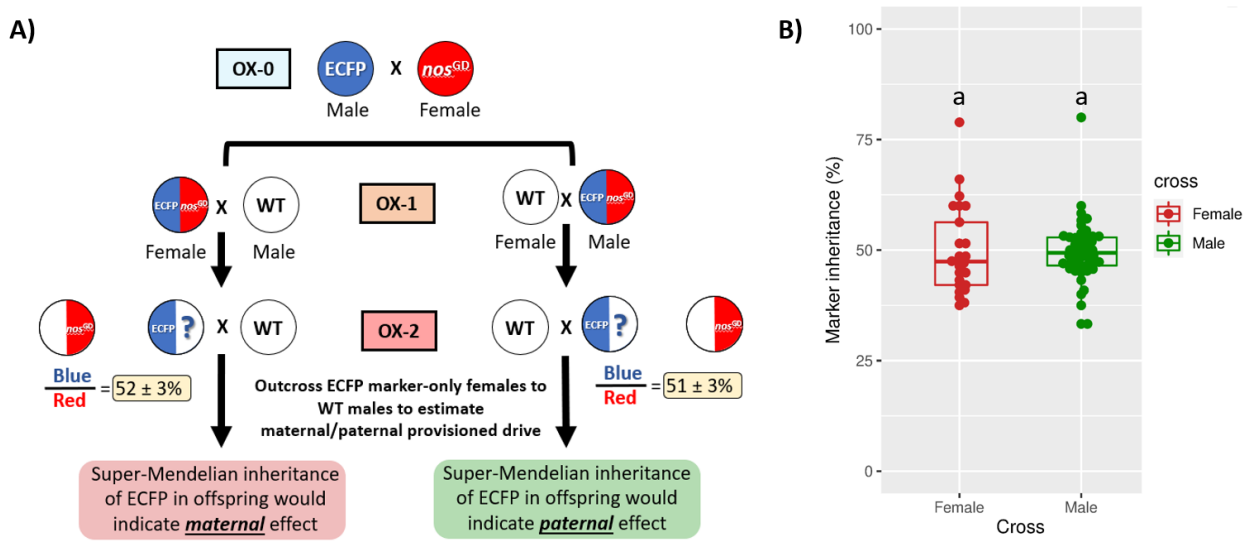

Figure 5. Locus balancing of an eCFP marker harboring line against the mCherry-marked AeaNosC109^{GD} line to test for parental GD effects. A) Crossing schematic for establishing trans-heterozygotes parentals (OX-1), which were then outcrossed to non-transgenic HWE mosquitoes to obtain the eCFP parentals for OX-2. The eCFP parentals used for OX-2 contained the eCFP marker in the Carb109 locus, allowing for drive into a non-transgenic allele if trans-acting Cas9-RNP was provisioned either maternally or paternally. B) eCFP marker inheritance for the final outcrossing of OX-2 to non-transgenic, where inheritance > 50% is suggestive of parentally supplied Cas9-RNP. Each data point in (B) represents the percentage of transgene inheritance resulting from the offspring of the second outcrossing of eCFP positive females to non-transgenic HWE males. The bar inside the box plot represents the median value, while the lower and upper borders of the boxes represent Q1 and Q3, respectively. Groups superseded by the same letter are not significantly different ($p > 0.05$). A minimum of 20 larvae was set for each group in order to be scored.

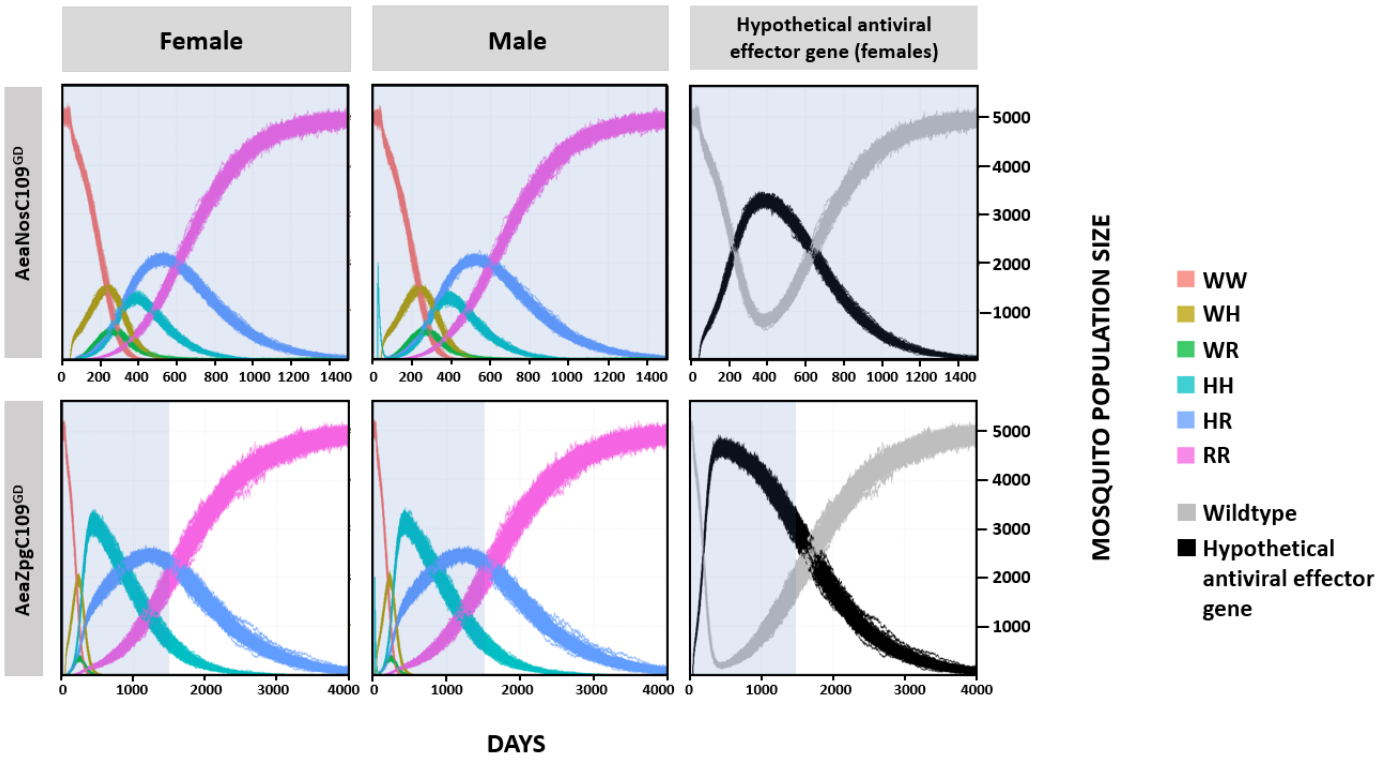

1179

1180 **Figure 6. Population modeling for the AeaNosC109^{GD} line (upper panels) and the**
1181 **AeaZpgC109^{GD} line (lower panels) using MGDrivE.** W = wildtype unedited allele, H = homing GD
1182 allele, R = GDBI resistance allele. A hypothetical refractory antiviral allele linked to the GD,
1183 shown as black in the right panels, displays the numbers of females in the population carrying at
1184 least one copy of the GD and a linked hypothetical 'antiviral effector gene'. The time scale in
1185 days differs for the two transgenic lines with the pale blue backshading representing 1500 days
1186 post-release (PR) for comparison.

1187

1188

1189

1190

1191

1192

1193

1194

1195

1196 **TABLES**

1197

1198 **Table 1. Active CRISPR/Cas9 target sites proximal to the original TIMP-P4 and Carb109**
1199 ***mariner/Mos1* insertion loci.**

Locus	sgRNA number	Genomic locus (distance from original *mariner/Mos1* insertion site)	Activity (# embryo pools / total pools)
TIMP-P4	sgRNA #5*	2: 321382225 (623 bp)	Active (3/3)
Carb109	2	3: 409717866 (19942 bp)	Not active (0/3)
	4	3: 409723215 (25291 bp)	Not active (0/3)
	6	3: 409699241 (1317 bp)	Not active (0/3)
	15	3: 409699138 (1214 bp)	Active (3/3)
	21	3: 409699885 (1961 bp)	Not active (0/3)
	29	3: 409699526 (1602 bp)	Not active (0/3)

1200 *Previously reported in Williams *et al.*, 2020 (17)

1201

1202

1203

1204

1205

1206

1207

1208

1209

1210

1211

1212

1213

1214

1215

1216 **Table 2. *Aedes aegypti* lines used in our study and respective injection efforts for their**
1217 **establishment.**

Line name	Marker	Purpose	Embryos injected	Survivors (F:M ; %)
Aeaβ2tT4^{GD}	3xP3 mCherry	GD at TIMP-P4 locus	1115	72 (31:41 ; 6.5%)
AeaNosT4^{GD}	3xP3 mCherry	GD at TIMP-P4 locus	959	154 (66:88 ; 16%)
Aeaβ2tC109^{GD}	3xP3 mCherry	GD at Carb109 locus	882	122 (64:58 ; 13%)
AeaNosC109^{GD}	3xP3 mCherry	GD at Carb109 locus	912	206 (90:116 ; 23%)
AeaZpgC109^{GD}	3xP3 mCherry	GD at Carb109 locus	568	45 (17:28 ; 7.9%)
AeaeCFPC109	3xP3 eCFP	Genetic balancer for Carb109 locus	1142	44 (24:20 ; 3.9%)

1218
1219
1220
1221
1222
1223
1224
1225
1226
1227
1228
1229
1230
1231
1232
1233
1234
1235

1236 **Table 3. Testing of non-transgenic offspring from OX-1 individuals to assess for the presence of**
1237 **GD blocking indels (GDBI) among the GD lines.**

Line	GD Parental	GD inheritance rate (% marker inheritance; n total)	Number of GD-negative larvae with indels / total number of GD negative larvae assessed (%)
AeaNosT4^{GD}	Male	Low (45.9%; 290)	0/40 (0%)
		High (58.1%; 136)	0/40 (0)
	Female	Low (42.9%; 163)	0/40 (0)
		High (51.3%; 117)	0/40 (0)
AeaNosC109^{GD}	Male	Low (55.3%; 228)	9/54 (16.7)
		High (86.4%; 214)	7/27 (25.9)
	Female	Low (61.5%; 148)	7/46 (15.2)
		High (89.7%; 136)	7/12 (58.3)
AeaZpgC109^{GD}	Male	Low (56.5%; 232)	0/41 (0)
		High (59.2%; 228)	0/51 (0)
	Female	Low (57.1%; 98)	2/27 (7.4)
		High (73.7%; 118)	1/23 (4.3)
Aeaβ2tC109^{GD}	Male	no GD (50.7%; 138)	0/10 (0)
	Female	no GD (52.5%; 40)	0/10 (0)

1238

1239

1240

1241

1242

1243

1244

1245

1246

1247

1248

1249

1250 **Table 4. Embryos injected for maternal contribution testing and the resultant genotype**
1251 **frequencies of surviving larvae used for CRISPR/Cas9 activity assessment.**
1252

Cross	Rep	Embryos injected	Surviving larvae N, (% of injected)	eCFP N, (% of larvae)	mCherry N, (% of larvae)
[AeaNosC109^{GD} x	1	1056	26 (2.4)	14 (53.8)	12 (46.1)
AeaeCFPC109]	2	1017	33 (3.2)	18 (54.5)	15 (45.5)
	3	1170	24 (2.0)	14 (58.3)	10 (41.7)
	1	1007	23 (2.3)	13 (56.5)	10 (43.5)
[AeaZpgC109^{GD} x	2	1015	26 (2.6)	12 (46.1)	14 (53.8)
AeaeCFPC109]	3	1004	46 (4.6)	22 (47.8)	24 (52.2)

1253

1254